Article

Discovery Medicine 2026; 38(207): 1230–1250
https://doi.org/10.24976/Discov.Med.202638207.98

The Amyloid β Precursor Protein-CD74 Axis Mediates Intercellular Communication Between *GABBR1*^{hi}*CHRM3*^{hi} Neuron-like Cells and *RYR1*$^{+}$*ESRRG*$^{+}$*BICC1*$^{+}$ Macrophages, Influencing Inflammatory Responses in Diabetic Nephropathy

Juan Li[1,†], YanLi Zhou[1,†], HuiYuan Li[1], Wei Feng[1], ZePei Qiu[1], HuanHuan Chen[1], XuFang Wu[1], JiaEr Ke[1], HaiQi Qin[2], XiangXin Meng[1,*]

[1]Department of Nephrology and Rheumatology, The Affiliated TCM Hospital of Guangzhou Medical University, The Affiliated Guangzhou Hospital of TCM of Guangzhou University of Chinese Medicine, 510630 Guangzhou, Guangdong, China
[2]The Second Clinical College of Guangzhou University of Chinese Medicine, 511400 Guangzhou, Guangdong, China
*Correspondence: 18022868737@163.com (XiangXin Meng)
[†]These authors contributed equally.
Submitted: 24 October 2025 Revised: 15 January 2026 Accepted: 22 January 2026 Published: 20 April 2026

Background: In the past decade, it has been established that dynamic communication exists among nerves, macrophages, and podocytes (PODO) within the kidney, which plays a crucial role in renal homeostasis and the response to acute and chronic renal injury. However, the exact molecular mechanisms of the interplay among these three elements in the progression of diabetic nephropathy (DN) remain to be elucidated. The aim of this study is to explore the intercellular communication via signaling molecules among neurons, macrophages, and PODO, and to determine their mechanism of action in renal inflammation in DN.
Methods: Multiple DN-related single-cell transcriptome sequencing datasets were merged. Using the Seurat pipeline, cells were standardized, underwent principal component analysis (PCA), dimensionality reduction, clustering, and annotation. Cells transmitting neural signals, macrophages, and PODO were identified using biomarkers from CellMarker 2.0 and SingleR method. The interactions of ligand-receptor pairs between these cells were analyzed using Celltalker and CellphoneDB. Additionally, differentially expressed genes (DEGs) in macrophages, and PODO in DN were obtained and annotated for Gene Ontology and Kyoto Encyclopedia of Genes and Genomes functions.
Results: A total of 2394 cells from kidneys exhibiting transcriptome characteristics highly similar to neurons were identified. These neuron-like cells were clustered into 11 cell clusters. Among these, cluster 7 (*GABBR1*^{hi}*CHRM3*^{hi}) showed a significant decrease in relative proportion in DN tissue ($p < 0.05$). A total of 202 macrophages were identified, clustered into 4 cell clusters. Notably, cluster C3 (*RYR1*$^{+}$*ESRRG*$^{+}$*BICC1*$^{+}$) was significantly reduced in DN. Functional analysis indicated that *RYR1*$^{+}$*ESRRG*$^{+}$*BICC1*$^{+}$ macrophages were associated with negative regulation of inflammatory responses. Cell communication analysis further revealed weakened interactions between *GABBR1*^{hi}*CHRM3*^{hi} neuron-like cells and *RYR1*$^{+}$*ESRRG*$^{+}$*BICC1*$^{+}$ macrophages involving Amyloid β precursor protein (*APP*)-*CD74*. Additionally, interactions of PODO with *RYR1*$^{+}$*ESRRG*$^{+}$*BICC1*$^{+}$ macrophages involving *SLIT1-ROBO2*, *EFNA5-EPHA4*, and *PDGFB-PDGFRB* were weakened, as was the interaction of *GABBR1*^{hi}*CHRM3*^{hi} neuron-like cells involving *VEGFA-FLT1*.
Conclusion: In DN, there is signal crosstalk between *GABBR1*^{hi}*CHRM3*^{hi} cells, anti-inflammatory phenotype macrophages, and PODO. The communication between these cells is primarily mediated through signaling pathways such as *APP-CD74*, *PDGFB-PDGFRB*, and *VEGFA-FLT1*.

Keywords: diabetic nephropathy; neural signals; renal macrophage; podocyte; amyloid β precursor protein; CD74; single-cell transcriptome sequencing

Introduction

Diabetic nephropathy (DN) is a common complication of diabetes, characterized by proteinuria, glomerulosclerosis, and renal fibrosis, and often leads to end-stage renal failure and poses a significant global health threat [1]. The pathology of DN centrally involves podocytes (PODO) injury. PODO, highly specialized cells, are crucial for maintaining the glomerular filtration barrier. They attach to the outer surface of the glomerular basement membrane (GBM) and, along with vascular endothelial cells, constitute an essential component of the glomerular filtration barrier. PODO regulate glomerular filtration by dynamically altering the size of filtration slits and the area of the membrane through contraction and expansion of their cell processes. Injury and loss of PODO lead to increased slit pore size and filtration membrane damage, resulting in albumin leakage into urine, which directly contributes to proteinuria and glomerulosclerosis in DN [2–4].

Substantial evidence indicates that PODO injury and loss in DN closely relate to renal macrophage-mediated inflammatory responses and impaired phagocytic activity [5, 6]. Renal biopsies from diabetic patients have demonstrated the co-localization of PODO and macrophages within the glomeruli [6,7]. Notably, significant macrophage infiltration is observed in the glomeruli of DN, correlating with elevated levels of proteinuria and renal interstitial fibrosis scores [8,9]. Additionally, *in vitro* studies of PODO and experiments using db/db mouse models of diabetes have indicated that macrophages accumulation and activation contribute to the reduction or loss of PODO processes and enhanced PODO apoptosis [10]. This phenomenon is attributed to the recruitment and activation of macrophages at renal injury sites in a high-glucose environment, accompanied by the secretion of inflammatory cytokines such as interleukin (IL)-1 beta (IL-1β), IL-2, IL-6, and tumor necrosis factor (TNF)-alpha (TNF-α) [6,11]. These cytokines adversely affect renal proteins and actin produced by PODO, stimulating the production or inhibiting the degradation of matrix proteins (e.g., type IV collagen). These matrix proteins, as crucial components of the PODO extracellular matrix (ECM), play key roles in maintaining foot process structure and cell adhesion, thus impacting the vitality and function of PODO. Protein expression imbalances lead to PODO damage, resulting in proteinuria, glomerulosclerosis, and renal fibrosis. Conversely, inhibiting macrophages infiltration can suppress the expression of pro-inflammatory genes, reduce monocyte and type IV collagen adhesion, and help maintain the morphology and survival of PODO. Additionally, damaged or apoptotic PODO release damage-associated molecular patterns, which are recognized by macrophages, further exacerbating the inflammatory response and amplifying renal damage.

Most studies on PODO injury have primarily focused on bone marrow (BM)-derived monocytes (BMMOs) as the source of macrophages, which are recruited to the lesion via the bloodstream under pathological conditions. However, with advances in renal macrophage lineage tracing and fate mapping studies, it has been discovered that macrophages in the kidney also originate from embryonic progenitors. These macrophages first colonize the kidney and persist in the tissue, undergoing self-renewal and maintenance through *in situ* proliferation, and are referred to as tissue-resident macrophages (TMs) [12–14]. Recent studies have also identified contributions of BMMO-derived macrophages to the TMs pool [14]. TMs exhibit distinct ecological distributions, phenotypic and functional characteristics from monocytes, contributing more significantly to antigen clearance and fibrosis in the kidney. Advances in single-cell sequencing of mouse and human renal tissues have revealed different subgroups of TMs in the kidney, each with specific markers and gene expression profiles, playing various roles in the progression of kidney injury in DN [15,16]. The current characterization of TMs lacks clear standards. In research, they are still traditionally categorized into classically activated M1 and alternatively activated M2 types. M1 and M2 play opposing roles, with M1 primarily regulating antigen presentation and immune inflammation, while M2 releases cytokines that inhibit inflammation or promote wound healing and tissue repair. Under conditions of persistent inflammation, M2 assumes a pro-fibrotic role [17,18]. Depending on the level of inflammation and/or the environment at the site of renal injury, macrophages can change their phenotype or express mixed, pro-fibrotic phenotypes [13]. For example, in a long-term high-glucose environment and oxidative stress, the kidney activates SK1, leading to an increase in renal sphingosine-1-phosphate (*S1P*). *S1P* activates macrophages *in vitro*, promoting renal epithelial cell proliferation and healing [19, 20]. Damaged kidneys express high levels of macrophage-migration inhibitory factor (*MIF*), which, in turn, activates $CD74^{+}$ macrophages [21]. The enhanced antigen presentation capability of macrophages, subsequently activating T lymphocytes, contributes to the onset of inflammation. In summary, the remodeling of macrophages in response to microenvironmental changes leads to complex roles and mechanisms in PODO injury in DN.

In the kidney, in addition to PODO, mesangial cells, and epithelial cells, neurotransmitters released from nerve fiber terminals also play a crucial role in regulating the phenotypic remodeling of macrophages. Neurons within the kidney encompass both sympathetic and parasympathetic nerves, distributed throughout the vascular plexus in areas such as the glomeruli and renal interstitium. Renal nerves are responsible for controlling glomerular perfusion and filtration functions. Furthermore, the autonomic nervous system is known to exert hemodynamic effects that impact both renal and immune functions [22]. Studies have demonstrated that denervation renders the kidneys more susceptible to lipopolysaccharide (LPS) and

antibody-induced nephritis [23]. Other research has shown that complete renal denervation can reduce monocyte influx into the nerves and decrease the levels of inflammatory cytokines, thus alleviating inflammation [24]. These findings suggest a potential role of neurons in renal inflammatory responses [25,26]. Additionally, in models of hypertensive disease, catecholamines (monoamine neurotransmitters) have been found to promote the accumulation of monocytes/macrophages, exacerbating renal inflammation and damage [27]. In models of acute kidney injury and IgA nephritis induced by unilateral renal ischemia-reperfusion, renal sympathetic nerves and peptidergic afferent nerve fibers release substances such as substance P (*SP*) and Calcitonin Gene-Related Peptide (CGRP), which recruit mononuclear macrophages and mediate renal inflammation [28,29]. In the mouse model with TM depletion established by Zhu Q *et al*. [30], specific TM depletion led to decreased distribution and tension of renal sympathetic nerves, reduced renin secretion, and an increased glomerular filtration rate. Supplementation with the neurotransmitter norepinephrine could rescue the TM depletion phenotype. This study confirmed the dynamic interaction between renal sympathetic nerves and TMs. Therefore, neurons in the kidney may mediate the phenotypic remodeling of macrophages through signal communication with macrophages, thereby regulating inflammatory responses. The key signals between neurons and TMs are not yet clear. Moreover, although some studies have identified neural cell clusters in embryonic kidney tissues, the cellular landscape in adult kidneys is different. In adult kidneys, projections of sympathetic and parasympathetic nerve fibers from the spinal cord lack complete transcriptomic information, making it challenging to identify neural fibers using single-cell RNA sequencing (scRNA-seq) technology. Therefore, this study utilizes single-nucleus transcriptome sequencing (snRNA-seq) data from renal tissues of patients with DN to identify TMs, PODO, and kidney cells exhibiting neural-like transcriptional features. The interactions and mechanistic impact of these neural-like clusters, expressing neural proteins, on TM function are analyzed. Additionally, we explore key proteins involved in TM-mediated PODO injury, indirectly elucidating the mechanisms by which neural inputs influence renal TM polarization and their impact on PODO damage in DN.

Methods

Acquisition and Preprocessing of Single-cell Sequencing Data

Human DN-related snRNA-seq were obtained from the GEO database, including GSE131882, GSE151302, GSE195460, GSE118184, and GSE114156. A total of 15 renal tissue samples were collected, comprising 5 DN samples (from GSE131882 and GSE195460) and 10 non-DN samples (from GSE151302, GSE118184, and GSE114156) (**Supplementary Table 1**). Non-DN samples were sourced from voluntarily donated healthy renal tissues. No significant differences in gender or age were observed between the non-DN and DN groups. Using the Seurat package (v4.3.0.1, Satija Lab, New York Genome Center, New York, NY, USA) in R software, we merged and processed multiple datasets, resulting in over 100,000 cells. Cells with a total gene count (nFeature_RNA) less than 200 or greater than 5000, and those with mitochondrial and ribosomal gene proportions exceeding 10% and 25% respectively, were filtered out. Ultimately, over 74,442 cells were included in our study. The average total gene count and the total number of molecules per cell in renal cells were 1765.42 $\pm$ 1134.49 and 7291.87 $\pm$ 14,563.17. The mitochondrial and ribosomal gene proportions of cells were 1.04% $\pm$ 2.38% and 5.34% $\pm$ 5.32%. Cells were then normalized the cells, and highly variable genes were extracted using the NormalizeData, FindVariableFeatures, and ScaleData functions. Principal Component Analysis (PCA) was performed based on 3000 high variability genes. Additionally, batch effects between different datasets were removed using the Harmony package (v0.1.1, Broad Institute of MIT and Harvard, Cambridge, MA, USA). The resulting normalized expression matrix, saved in a sparse matrix named "data", was utilized for subsequent cell clustering and annotation analyses.

Cell Clustering and Annotation

To analyze the classification and transcriptional characteristics of renal cells in patients with DN, the K-nearest neighbor distances between cells were calculated based on the top 20 principal components (PCs) post-batch removal using the FindNeighbors function, and cell clustering was performed using the FindClusters function with a resolution parameter set to 0.8. Subsequently, dimensionality reduction using the RunUMAP function, and the results were visualized with the DimPlot function. To identify the cell types present in the kidneys, marker genes for each cell cluster were initially obtained using the FindAllMarkers function. The cells were then annotated based on biomarkers derived from the research of Parker C. Subsequently, we annotated the cells according to the biomarkers described by Yang *et al*. [31], as listed in the (**Supplementary Table 2**). Additionally, automatic annotation was conducted using the singleR package (v2.0.0, Icahn School of Medicine at Mount Sinai, New York, NY, USA), and kidney markers from the CellMarker (v2.0) database (http://117.50.127.228/CellMarker/) were used for validation.

Analysis of Neuron-like Cell Types and Functions

After cell annotation, a high degree of overlap was observed in the Uniform Manifold Approximation and Projection (UMAP) dimensional distribution between neuron-like and other renal cells such as tubular cells, PODO, and endothelial cells (ENDO). To further confirm the presence of

neuron-like cells in the renal tissues, single-cell RNA sequencing (scRNA-seq) datasets of cholinergic neurons, including GSE209947, GSE192405, and GSE213569, were introduced. Dimensionality reduction and clustering were repeated, and cells overlapping with cholinergic neurons expressing elav-like (*ELAVL) 3*, *ELAVL4*, and Sex Determining Region Y (SRY)-Box transcription factor (*SOX)* 11 were annotated as neuron-like cells and designated as a distinct cluster. Additionally, renal tissue neuron-like cells were predicted through semi-supervised clustering (1), AUCell enrichment (2), and Semi-Supervised Category Identification and Assignment (SCINA) analysis (3) based on neuronal marker transcriptional expression characteristics. The neuron-like cell clusters were then selected as a subset in Seurat for reanalysis with PCA, cell clustering, and UMAP dimensional reduction. The FindAllMarkers function was used to obtain markers for different cell clusters, thereby annotating phenotypes. The functions of different subtypes of neuron-like cells were analyzed using irGSEA (v1.1.3, Sun Yat-sen University Cancer Center, Guangzhou, China) and UCell (v2.0.1, University of Lausanne, Lausanne, Vaud, Switzerland). Furthermore, variations in the cellular proportion of different neuron-like cells subtypes between DN and control (CON) groups were statistically examined.

(1) Semi-supervised clustering was performed using the AddModuleScore function in the Seurat package, with the following formula (where n is the number of target genes g, and i is the number of background genes G):

$$\text{Neu\_score} = \sum_{k=1}^{n}(gk+\cdots+gn)/n-\sum_{k=1}^{i}(Gk+\cdots+Gi)/i$$

(2) AUCell scoring was calculated using the AUCell and irGSEA packages, with the methodology detailed at https://github.com/aertslab/AUCell.

(3) SCINA scoring was conducted using the SCINA (v1.2.0) package, with its principle detailed at https://github.com/jcao89757/SCINA.

Types and Functions of Immune Cells and Macrophages

PTPRC (*CD45*) was utilized to mark immune cells (IMC), and a total of 1971 cells were identified. Cells with high expression of *PTPRC* were selected as a subset in Seurat for reanalysis and annotation, and the proportional changes among different types of IMC were quantified. Recent studies have indicated significant macrophage infiltration in DN tissues and their involvement in disease progression. Therefore, subsequent research focused on macrophages. Cell clusters with significantly high expression of *CD163* and *MRC1* were annotated as macrophages. To ascertain the origin of renal macrophages, scRNA-seq data from peripheral blood mononuclear cells (PBMCs, *CD14*$^{+}$) and embryonic kidney tissues were additionally introduced. After batch removal using the Harmony function, PCA dimensional reduction was conducted with the RunPCA function, and lineage tracing analysis was performed using Monocle (v2.26.0, University of Washington, Seattle, WA, USA). Current fundamental research has recognized that macrophages exhibit various molecular subtypes and functions. Consequently, macrophages were selected, and the PCA, clustering, and UMAP dimensional reduction analyses were repeated for these cells. Molecular characteristics of different macrophage cell clusters were obtained using the FindAllMarkers function. The functions of different macrophage subtypes were analyzed using irGSEA and UCell. Differences in the proportions of various macrophage subtypes were also examined between the DN compared to the CON group.

Acquisition of Significantly Differentially Expressed Genes in Cells and Their Functional Enrichment Analysis

To elucidate potential molecular signals underlying functional abnormalities in neuron-like cells and macrophages in DN, the FindMarkers function and Likelihood-ratio test were employed to identify differentially expressed genes (DEGs) between various subtypes of neuron-like cells and macrophages in DN and CON groups. DEGs were selected based on the criterion of an adjusted *p*-value (*adj_p*) < 0.05. Subsequently, enrichment of these DEGs in Gene Ontology (GO) and Kyoto Encyclopedia of Genes and Genomes (KEGG) pathways was analyzed using the clusterProfiler (v4.6.2, Southern Medical University, Guangzhou, China), org.Hs.eg.db (v3.16.0, Fred Hutchinson Cancer Center, Seattle, WA, USA) packages, as well as gene set enrichment analysis (GSEA). Additionally, the STRING module in Cytoscape software (v3.9.1, Cytoscape Consortium, San Diego, CA, USA) was utilized to investigate the interactions among DEGs and to construct a protein-protein interaction network (PPI). Thereafter, core networks and central nodes within the PPI were identified using the Molecular Complex Detection (MCODE) plugin and the cytohubba plugin in Cytoscape (v3.9.1), thereby pinpointing key genes regulating neuron-like cells and macrophage injury in DN.

Pseudo-time Analysis

To investigate the dynamic changes in different cell clusters and subtypes of macrophages, pseudo-time analysis was conducted using the Monocle package based on cell cluster markers. Single-cell sequencing count data were loaded using the newCellDataSet function. Data were normalized using the estimateSizeFactors, and estimateDispersion functions, and dimensionality reduction was performed using the ReduceDimension() functions with the 'DDRTree' method, were used for the initialization and normalization of count data. Cells were ordered along a

pseudo-time trajectory using the OrderCells function. The DifferentialGeneTest function was employed to identify genes related to pseudotime. Additionally, Scanpy was utilized to calculate the Partition-based graph abstraction (PAGA) trajectory distribution of cells. This analysis ultimately revealed the differentiation time distributions across various cell subtypes.

Tight Communication Between Cells

To explore signal communication between different subtypes of neuron-like cells and renal macrophages, as well as between macrophages and PODO, ligands and receptors differentially expressed among neuron-like cells, macrophages, and PODO were initially identified. The Pearson correlation of expression for these ligands and receptors was then analyzed using celltalker (v0.0.7.9000, University of Pittsburgh, Pittsburgh, PA, USA) and CellphoneDB (v5.0, Wellcome Sanger Institute, Cambridge, UK). The statistical significance of these correlations was assessed using the Wilcoxon test.

Co-culture of GABBR1^{hi}CHRM3^{hi}Neuron-like Cells With RYR1^{+}ESRRG^{+}BICC1^{+}Macrophages

GABBR1^{hi}CHRM3^{hi} neuron-like cells were treated with high glucose (HG; 30 mM D-glucose) for 24 h. The cell culture supernatant (CCS) was then collected and used to treat *RYR1^{+}ESRRG^{+}BICC1^{+}* macrophages for another 24 h.

Flow Cytometry

The treated cells were collected and incubated with an anti-CD74 primary antibody at a 1:50 dilution. Subsequently, a fluorophore-conjugated secondary antibody (Alexa Fluor 488-conjugated goat anti-mouse IgG (A28175, Thermo Fisher Scientific)) was added and incubated. After each step, cells were washed with PBS and centrifuged. All operations were conducted on ice and protected from light. Ultimately, cells were analyzed using an LSR Fortessa X-20 cell analyzer (BD Biosciences). Data were acquired in FCS format and analyzed using FlowJo software (version 10).

qRT-PCR

Total RNA was isolated from cultured cells using Trizol reagent (Ambin, 411502). Hifair III 1st strand cDNA Synthesis SuperMix (Yeasen, H8223900) was used to synthesize cDNA from 1 µg of total RNA following the manufacturer's instructions. In addition, qRT-PCR was conducted with diluted cDNA, gene-specific primers, and Hieff qPCR SYBR Green Master Mix (Yeasen, H2306210). The thermocycling conditions were set according to the manufacturer's instructions, and relative mRNA levels of target gene were calculated using the $2^{-\Delta\Delta CT}$ method.

The primers used in this study were as follows: APP (forward AACCCCAGATTGCCATGTTCT, reverse GCAGTTCAGGGTAGACTTCTTGG), CD74 (forward GGCAACATGACAGAGGACCA, reverse GCTCTCACATGGGGACTGG), GAPDH (forward AAGGGTCATCATCTCTGCCC, reverse CATGGACTGTGGTCATGAGT).

Western Blot

Cells were harvested and homogenized on ice using RIPA lysis buffer (Beyotime, P0013C) containing a 1:100 dilution of protein phosphatase inhibitor (Solarbio, P1260) and a 1:100 dilution of PMSF solution (Beyotime, ST507). After centrifugation at 12,000 rpm for 20 min at 4 °C, protein concentrations in the supernatant were determined by BCA assay (Solarbio, PC0020) according to the manufacturer's instructions. Equal amounts of protein were boiled in sodium dodecyl sulfate-polyacrylamide gel electrophoresis (SDS-PAGE) protein loading buffer (Yeasen, S3301100) for 5 min, and subjected to 8%–12% SDS-PAGE gels and then transferred to PVDF membranes (Immobilon, R1PB81493). The membranes were blocked with 5% skimmed milk, washed with TBS-T, incubated with primary antibodies, and subsequently incubated with corresponding horseradish peroxidase (HRP)-conjugated secondary antibodies (31460, Thermo Fisher Scientific). Protein bands were visualized using ECL chemiluminescent reagent (Meilunbio, MA0186-1).

Antibodies used in the present study include: anti-GAPDH (Proteintech, 10494-1-AP), anti-APP (PTM-biolab, PTM-20007) and anti-CD74 (PTM-biolab, PTM-6631), HRP-conjugated goat anti-rabbit IgG (Proteintech, SA00001-2), and HRP-conjugated goat anti-mouse IgG (Proteintech, SA00001-1).

Co-immunoprecipitation (Co-IP)

The Co-IP Pierce™ kit (88804, Thermo Fisher Scientific, USA) was used in accordance with the manufacturer's instructions, with all procedures performed on ice. The APP primary antibody was added to the protein lysate samples, and the mixtures were incubated overnight at 4 °C. Subsequently, Pierce™ Protein A/G Agarose Beads were added to the reaction mixtures, followed by incubation for 2–4 h at 4 °C. After incubation, the bead-protein-antibody complexes were collected by centrifugation and washed three times with ice-cold Wash Buffer. The immunoprecipitated complexes were then eluted using the elution buffer. Finally, the eluted samples were subjected to Western blot analysis.

Statistical Methods

Analysis and visualization of snRNA-seq and scRNA-seq data were conducted using the R software (v 4.2.2) and RStudio (v2022.12.0+353). The likelihood-ratio (L-R) test was utilized to detect the significance of gene ex-

pression differences. The Wilcoxon rank-sum test was employed to assess the significance of cell proportions, gene expression levels, and UCell enrichment scores. Student's *t*-test was used to assess the statistical significance of Pearson correlation coefficients between ligands and receptors. The Benjamini-Hochberg method was applied to adjust *p*-values, yielding false discovery rate (*FDR*) or adjusted *p*-values (*adj-p*). And *FDR*, *p*-value or *adj-p* < 0.05 were considered statistically significant, indicating meaningful differences between groups.

Results

Abnormal Reduction of GABBR1^{hi}CHRM3^{hi} Cells in Diabetic Nephropathy

A total of 13 cell types were identified from human kidneys, annotated as renal tubules (proximal tubules (PT), distal convoluted tubules (DCT), proximal thick limb tubules (TAL)), PODO, ENDO, IMC, among others (**Supplementary Fig. 1** and **Supplementary Fig. 2A**). Overall, PT accounted for the highest relative proportion (29.72%), followed by TAL (15.81%) and DCT (18.18%) (**Supplementary Fig. 2B,C** and **Supplementary Table 3**). Cell types in renal tubules, primarily including epithelial cells and neurons, were further annotated using singleR (**Supplementary Fig. 3**).

To further identify neurons, the scRNA-seq dataset of neurons was introduced (**Supplementary Table 1**). Neurons and renal cells were observed to overlap in the Harmony dimensionality reduction distribution (**Supplementary Fig. 4A–J**), indicating the presence of cells with similar transcriptional characteristics. These cells expressed *ELAVL4*, *STMN2*, *SYT1*, *NES*, among others (**Supplementary Fig. 4K–T** and **Supplementary Fig. 5**). Subsequently, neurons were identified using semi-supervised clustering, AUCell scoring, and SCINA methods, with corrections applied based on neuron-related scRNA-seq datasets. Results revealed that semi-supervised clustering based on neuronal marker expression characteristics (**Supplementary Table 4**, **Supplementary Fig. 6A,B**, $p < 0.001$) and AUCell (**Supplementary Fig. 6C,D**, $p < 0.001$) were used to score individual cells as neurons, with scores from the neuronal datasets being significantly higher than those of the renal datasets, and the distribution of score density consistent with the UMAP dimensionality reduction distribution of neuronal cells (**Supplementary Fig. 6G**). Notably, in semi-supervised clustering, the accuracy of neuron scoring reached 92% (**Supplementary Fig. 7A**), while other methods scored less than 50% (**Supplementary Fig. 7B,C**). However, the SCINA method showed that the average neuronal score of kidney cells was significantly higher than that of the neuronal datasets (**Supplementary Fig. 6E,F**, $p < 0.001$). Additionally, neurons predicted by the AUCell method were found to include previously annotated cell types such as immune cells across all kidneys samples (**Supplementary Fig. 7D–F**), rendering the results uninformative. The accuracy of the SCINA method in annotating neurons was 96% (**Supplementary Fig. 7G–I**), slightly lower than the 97% of the semi-supervised method, although the distribution of annotated neuron scores did not align with the actual distribution of neurons in the reference dataset (**Supplementary Fig. 6E,G**). Therefore, semi-supervised clustering was used for neuronal scoring of renal snRNA-seq, and cells with scores greater than 0 were selected for prediction as neurons (**Supplementary Fig. 8**). Given that the kidney primarily contains projections of nerve fibers, it was hypothesized that the renal cells predicted as neurons might actually represent subtypes of ENDO, PODO and other cell types. These cells exhibited transcriptional characteristics highly similar to neurons, expressed neuro-related genes and neurotransmitter receptors, and might function in neural signal transduction. This suggests a potential role of these renal cell types in neuronal-like signaling within the kidney.

In summary, using the semi-supervised method, 2714 neuron-like cells were obtained (**Supplementary Table 5**). After excluding *PTPRC*-expressing cells, 2394 neuron-like cells were included for subsequent analysis (DN vs CON = 894/1500). These cells were re-clustered into 11 cell clusters following dimensionality reduction (Fig. 1A). Re-annotation identified cell types (**Supplementary Table 6**), including cluster 7 (C7; *GABBR1^{hi}CHRM3^{hi}*, Fig. 1A,B and Fig. 2A), which showed a significantly reduced relative proportion in DN ($p < 0.05$, Fig. 1D). C7 predominantly represented a subgroup within the MES/ENDO clusters (Fig. 1C). Functional enrichment analysis revealed that the transcriptomic expression characteristics of *GABBR1^{hi}CHRM3^{hi}* cells were highly positively correlated with pro-inflammatory signals such as *IL2* and *TNFA* (Fig. 2B), suggesting a potential link between *GABBR1^{hi}CHRM3^{hi}* cells and the inflammatory response in DN.

Aberrant Up-regulation of Apoptotic Signaling in GABBR1^{hi}CHRM3^{hi} Cells in Diabetic Nephropathy

A total of 667 DEGs were further identified in *GABBR1^{hi}CHRM3^{hi}* cells in DN (Fig. 3A). And GSEA results of these DEGs revealed a significant decline in biological functions related to post-transcriptional gene expression regulation, cell-cell adhesion, as well as a notable decrease in negative regulation pathways of neuronal death in DN (Fig. 3B,C). Furthermore, construction of an interaction network involving these 667 DEGs revealed that genes related to neuronal apoptosis regulation and cell adhesion pathways were centrally located within the protein-protein interaction network (Fig. 4A). These findings indicated that *GABBR1^{hi}CHRM3^{hi}* cells might undergo abnormal changes in cell morphology and apoptosis. Notably, key proteins such as *PPARGC1A*, *CREBBP*, *FOXO3*, *PPARA*, *TLR4*, *NCOA2*, *CD36*, *APOE*, and *MED17* were

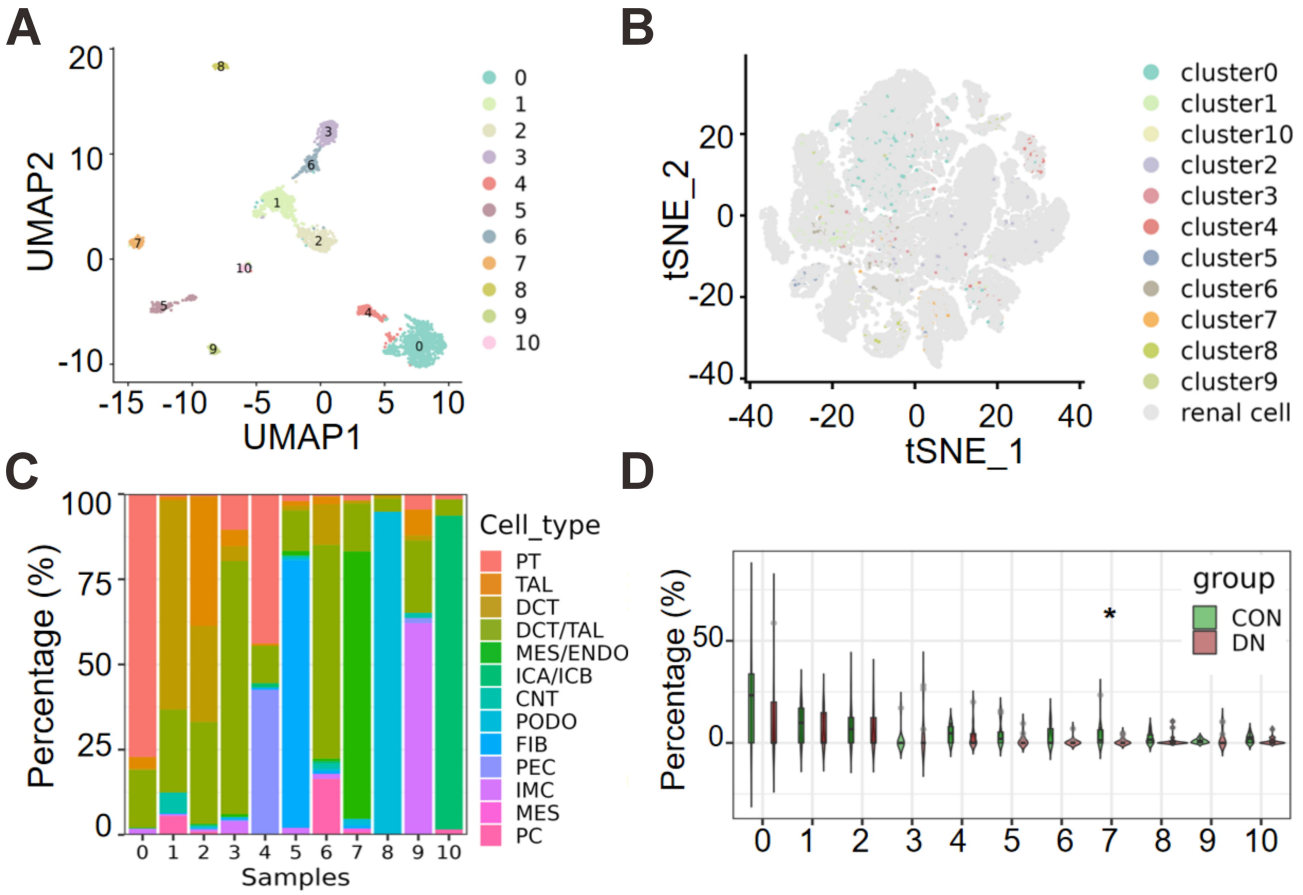

Fig. 1. Identification of neurons in diabetic nephropathy. (A) Renal neuron-like cells clustered and categorized into 11 clusters based on transcriptomic expression characteristics. (B) Renal tubular and immune cells re-annotated to renal neurons. (C) Relative distribution of renal neuron types. (D) The intergroup differences in the relative proportions of neuronal cells, with a significant reduction in *GABBR1*^{hi}*CHRM3*^{hi} neuron-like cells (annotated as C7) in comparison to the control (CON) group. * indicates a significant difference ($p < 0.05$) compared to the CON group.

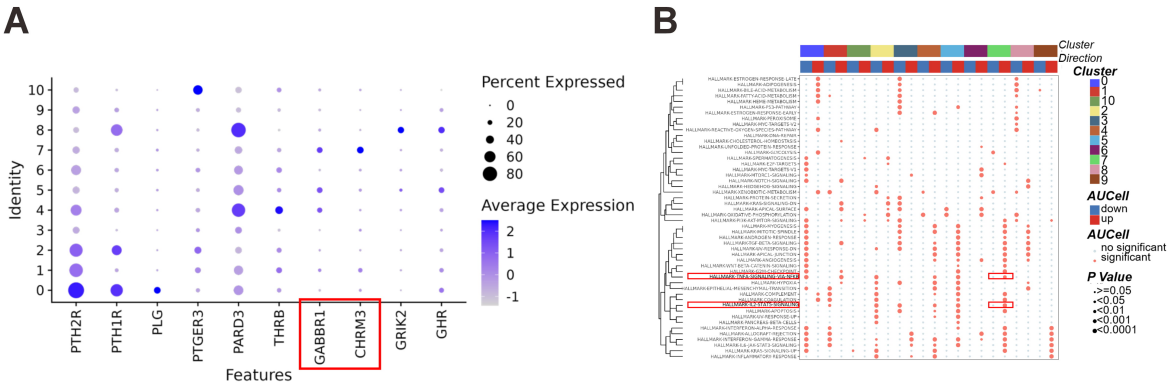

Fig. 2. Markers and functional enrichment of different types of neurons. (A,B) The expression of markers in different types of neurons (A) and their respective clusters (B).

identified as central proteins in the regulation of neuronal apoptosis pathways (Fig. 4B). This indicated that these proteins play a crucial role in regulating the apoptosis of *GABBR1*^{hi}*CHRM3*^{hi} cells and their adhesion or signaling interactions with other cells.

Increased Consumption of Tissue Resident Anti-inflammatory RYR1^{+}*ESRRG*$^{+}$*BICC1*$^{+}$ *Macrophages in Diabetic Nephropathy*

To further analyze the impact of *GABBR1*^{hi}*CHRM3*^{hi} cells dysfunction on macrophages in DN, it was essential to

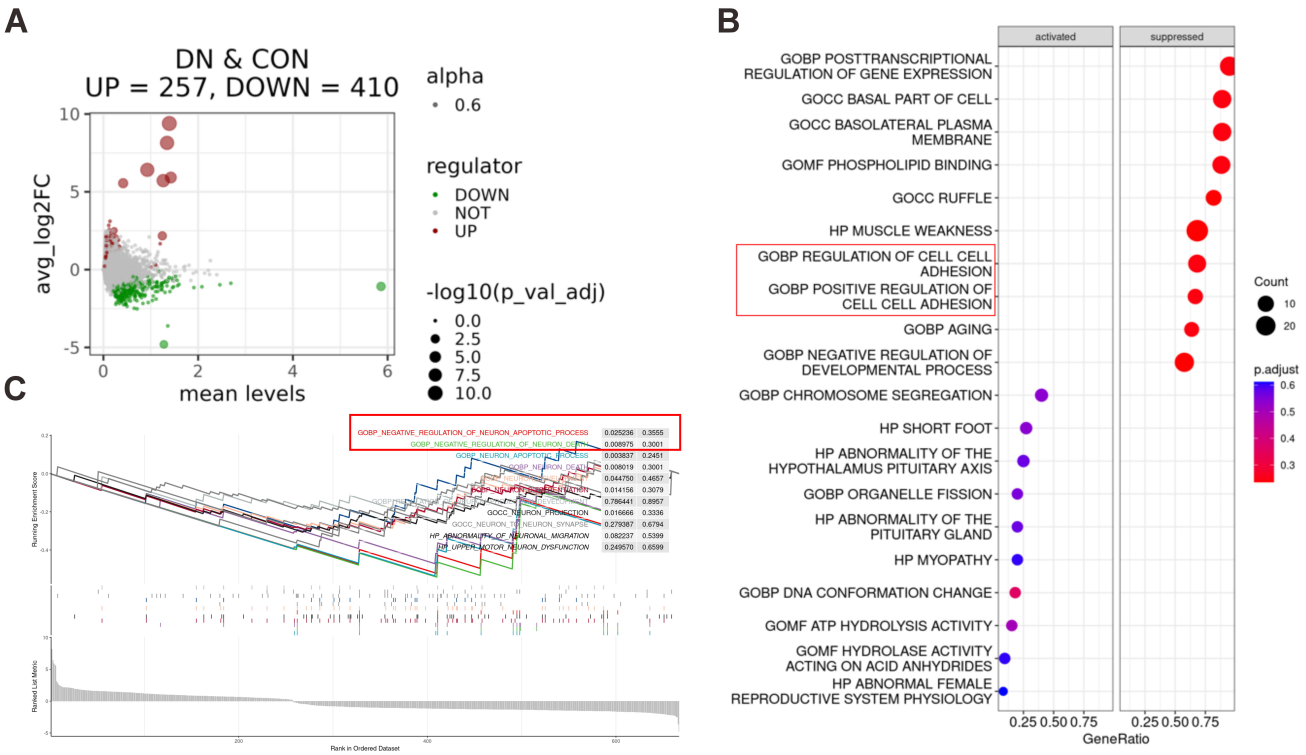

Fig. 3. Gene differential expression and enrichment analysis in *GABBR1*^{hi}*CHRM3*^{hi} neuron-like cells. (A) The volcano plot of gene differential expression in *GABBR1*^{hi}*CHRM3*^{hi} neuron-like cells. (B) Top 20 GSEA enrichment pathways for differentially expressed genes. (C) Enrichment results of neurologically related pathways.

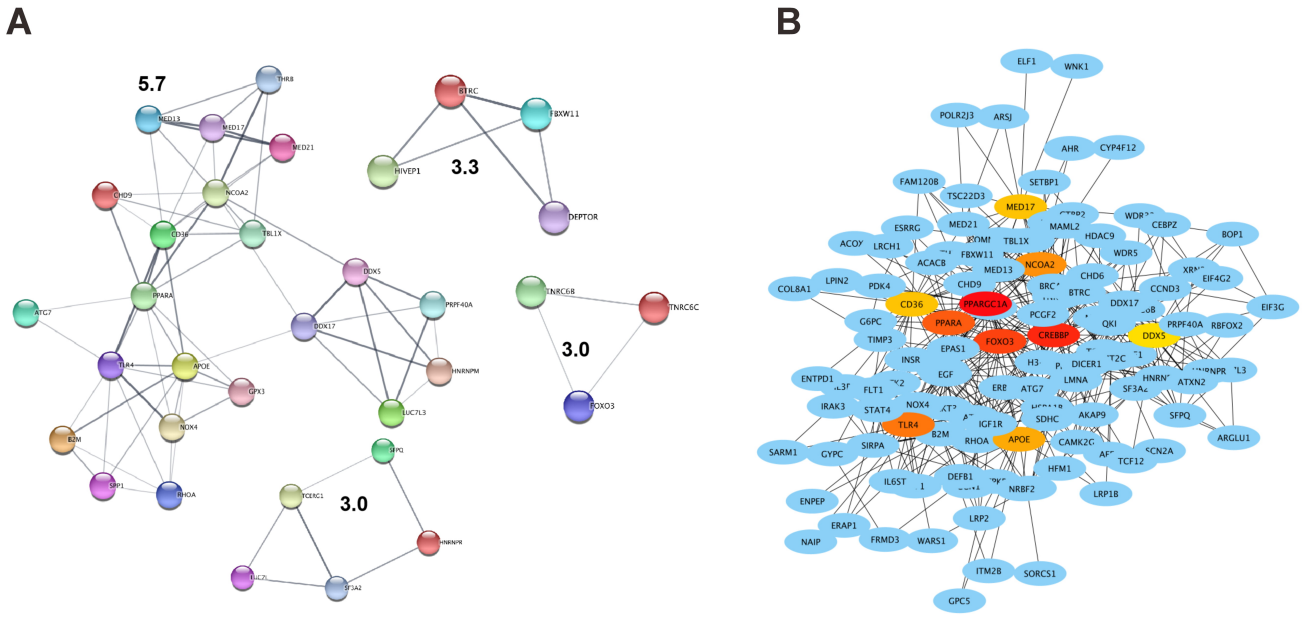

Fig. 4. Core genes regulating apoptosis and cell adhesion in *GABBR1*^{hi}*CHRM3*^{hi} neuron-like cells. (A) Key gene clusters calculated using the cytohubba-MCC (maximum group centrality) algorithm that regulate neuronal apoptosis and adhesion signaling. (B) Core genes calculated using the MCODE algorithm that regulate neuronal apoptosis and adhesion signaling.

identify and characterize macrophages present in DN tissues. Initially, we conducted an analysis of IMC in the kidney tissue (*PTPRC*, Fig. 5A) and clustered them into ten distinct clusters based on their transcriptomic features (Fig. 5B). These clusters were primarily annotated as B cells, T cells, and macrophages (Fig. 5C,D). Among these, T cells constituted the predominant cluster (Fig. 5D), with a relative increase in their proportion in DN samples, al-

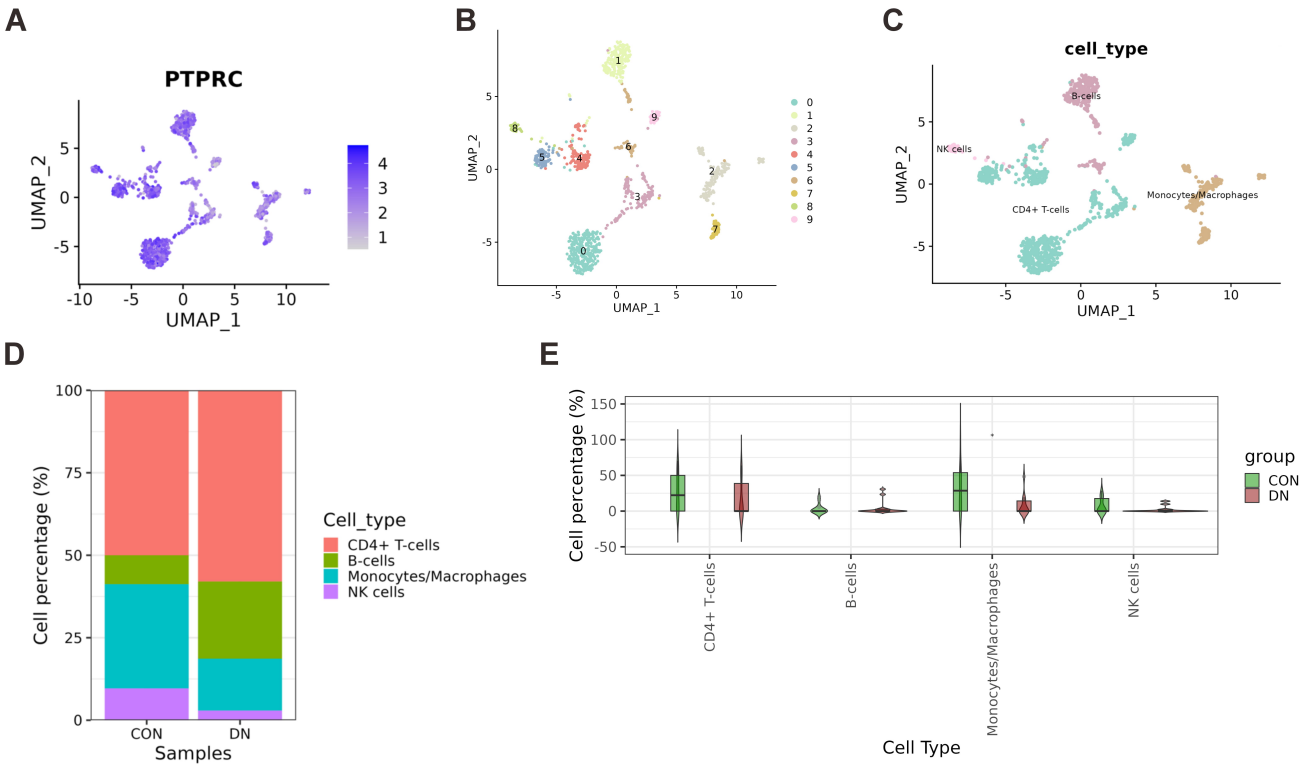

Fig. 5. Annotation of immune cells in renal tissue. (A) The expression distribution of the immune cell marker *PTPRC* after UMAP dimension reduction. (B) Clustering distribution of immune cells after UMAP dimension reduction, categorized into 10 clusters. (C) The annotation results for immune cells, including B cells, T cells, macrophages, and natural killer cells (NK). (D) The relative proportions of different immune cell types in DN. (E) Statistical results of relative proportions among different immune cell types, with statistical significance observed only in the relative proportion of macrophages. * indicates $p < 0.05$ compared with control (CON) group.

though this increase did not reach statistical significant (Fig. 5E). Interestingly, a significant decrease in the proportion of macrophages was observed in the DN group (Fig. 5E), a finding that contrasts with existing research.

To address these contradictory results and explore whether the origin and phenotype of macrophages might explain this discrepancy, the source of renal macrophages was analyzed. The analysis was supplemented with additional datasets, including pbmc3k, pbmc4k (PBMC), and GSE112570 (fetal kidney tissue, n = 2). PCA and dimensionality reduction based on gene transcription features clearly distinguished renal macrophages from PBMC and fetal kidney samples (**Supplementary Fig. 9A**). Macrophages originating from PBMC exhibited high expression levels of *CD14* (**Supplementary Fig. 9B**), *CD68* (**Supplementary Fig. 9C**), and *LYZ* (**Supplementary Fig. 9D**), while renal macrophages showed high expression of *PTPRC* (**Supplementary Fig. 9E**), *CD163* (**Supplementary Fig. 9F**), and *MRC1* (**Supplementary Fig. 9G** and **Supplementary Fig. 10**). Furthermore, pseudotime analysis to trace the lineage of renal macrophages revealed that renal macrophages originated from embryonic kidneys rather than PBMC (**Supplementary Fig. 11**).

In summary, a total of 202 TMs were identified in kidney tissues. Subsequent analysis of their phenotypes and functions in DN showed that macrophages in the kidney could be categorized into four clusters (Fig. 6A). Clusters C0 ($CD86^{hi}$) and C2 ($CD86^{hi}CD163^{lo}MRC1^{hi}$) exhibited a significant increase in the enrichment scores of inflammation-related pathways. In contrast, cluster C3 ($CD86^{lo}CD163^{hi}MRC1^{hi}$) displayed a significant decrease in the enrichment scores of inflammation pathways (Fig. 6B). Cluster C1 ($CD86^{lo}CD163^{lo}MRC1^{lo}$) exhibited a significant decrease in the enrichment scores of protein translation and cell metabolic capabilities (Fig. 6B). Notably, the relative proportion of C3 decreased significantly in the DN group (Fig. 6C), and this cluster specifically expressed *RYR1*, *ESRRG*, and *BICC1* (**Supplementary Fig. 12** and Fig. 7D–F), designated as $RYR1^{+}ESRRG^{+}BICC1^{+}$.

Using classical markers to indicate different macrophage cluster molecular phenotypes, the results indicated that *CD163* and *MRC1* (anti-inflammatory phenotype) were primarily enriched in clusters C2 and C3. In comparison to C3, C2 exhibited decreased expression of *CD163* and *MRC1* but showed high expression of the pro-inflammatory marker *CD86* (**Supplementary Fig. 11** and Fig. 7A–C). This suggested that C3 was functionally similar to the classical M2 phenotypes. Furthermore, pseudotime analysis based on macrophage marker genes (**Supplementary Fig. 13**) revealed that C1 (C1-1) rep-

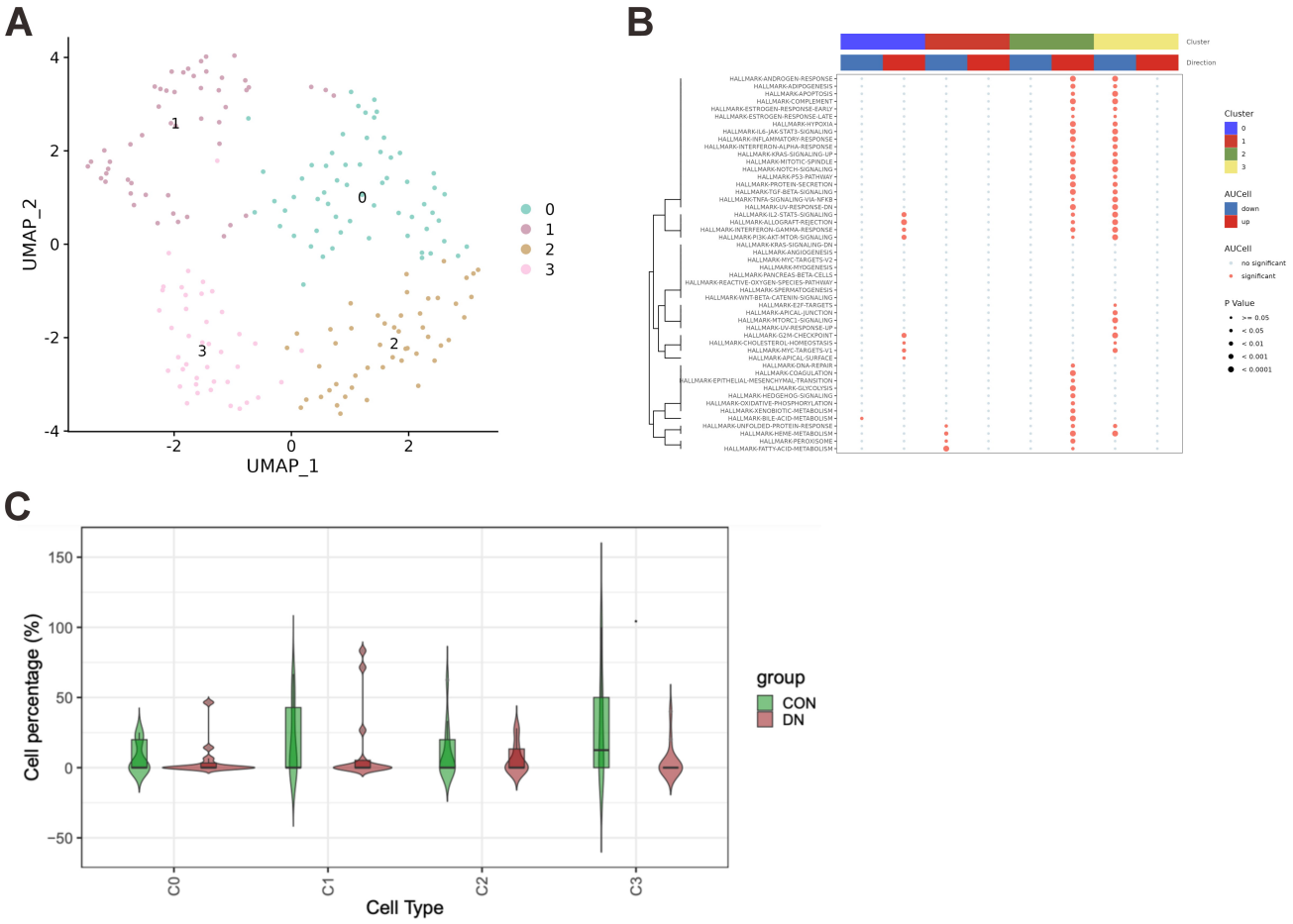

Fig. 6. Subtypes of renal macrophages in diabetic nephropathy. (A) The clustering results of renal macrophages, and the UMAP classification of different subtypes of macrophages. (B) Results of functional enrichment analysis for different types of macrophages. (C) Results of differential testing for the relative proportions of different macrophage types. * indicates $p < 0.05$ compared with control (CON) group.

resented the starting point for macrophage development, from which three differentiation trajectories emerged. Ultimately, these trajectories transitioned to C2 (C2-8) and C3 (C3-10 and C3-11) at differentiation nodes 1 and 4, respectively (Fig. 7G–I). C0 macrophages appeared to be a product of failed differentiation. These findings suggested that DN was primarily characterized by a reduction in *RYR1*$^{+}$*ESRRG*$^{+}$*BICC1*$^{+}$ macrophages.

GABBR1^{hi}*CHRM3*^{hi} *Cells Regulate RYR1*$^{+}$*ESRRG*$^{+}$*BICC1*$^{+}$ *Macrophages Polarization Through APP-CD74 Signaling in Diabetic Nephropathy*

To investigate the signaling communication between *GABBR1*^{hi}*CHRM3*^{hi} cells and *RYR1*$^{+}$*ESRRG*$^{+}$*BICC1*$^{+}$ macrophages, celltalker and cellphonDB were utilized to analyze the significant interactions between ligands and receptors expressed by these cells. Results from celltalker revealed that *GABBR1*^{hi}*CHRM3*^{hi} cells interacted with *RYR1*$^{+}$*ESRRG*$^{+}$*BICC1*$^{+}$ macrophages via *APP* on *GABBR1*^{hi}*CHRM3*^{hi}cells binding to CD74 on macrophages, as well as through PTPRM and CDH1 (Fig. 8A and **Supplementary Fig. 14**). These findings indicated a significant interaction between the two cell types.

Additionally, interactions involving *APP-SORL1*, *APP-TNFRSF21*, *VEGFA-NRP1*, and *COPA-CD74* were identified by CellPhoneDB (Fig. 8B and Fig. 9). Among these interactions, *APP* (Fig. 10A) and *CD74* (Fig. 10D) were widely expressed on the membranes of neuron-like cells and macrophages, with overall expression levels higher than those of other ligand-receptor pairs. These findings suggest that *APP-CD74* might play a dominant role in the communication between *GABBR1*^{hi}*CHRM3*^{hi} cells and *RYR1*$^{+}$*ESRRG*$^{+}$*BICC1*$^{+}$ cells.

Furthermore, compared with the CON group, the relative proportion of *APP*$^{+}$ neuron-like cells significantly decreased ($p < 0.05$, Fig. 10B,C), while the overall proportion of *CD74*$^{+}$ macrophages exhibited an increasing trend, although this difference did not reach statistical significance ($p > 0.05$, Fig. 10E,F).

Functionally, *APP* was found to regulate neuronal *MAPK* cascades, *VEGFA-VEGFR2* signaling, oxidative

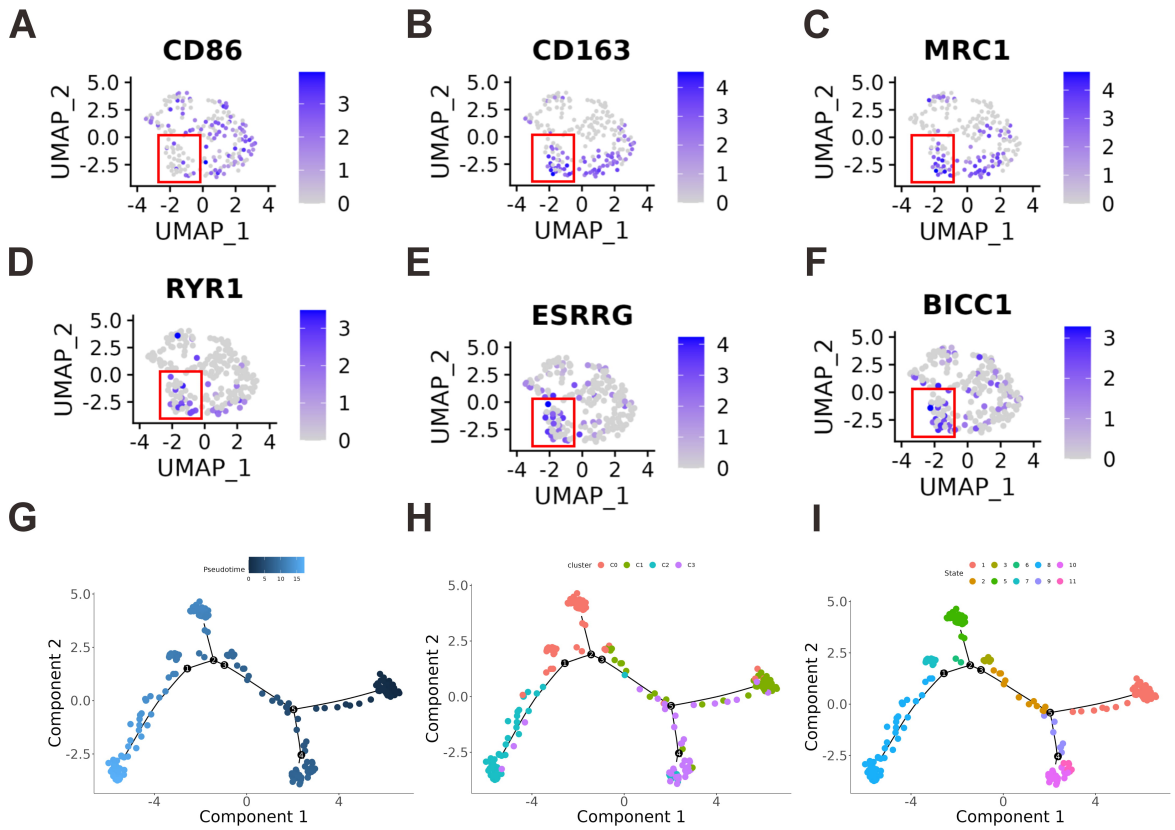

Fig. 7. States of different macrophage clusters. (A–C) The expression distribution of classical macrophage markers including *CD86* (A), *CD163* (B), and *MRC1* (C) in the kidney. (D–F) The specific expression of markers including *RYR1* (D), *ESRRG* (E), and *BICC1* (F) in macrophage cluster C3. (G–I) Results of pseudotime analysis for renal macrophages, showing the pseudotime states of single cells (G), different macrophage clusters (H), and differentiation stages (I). The red boxes indicate C3 macrophages.

stress, and cell-cell interactions, as shown in **Supplementary Fig. 15A,B**. In contrast, *CD74* predominantly regulated MHCII assembly and membrane localization, chemokine signaling in the immune system, as well as translation and ubiquitination of cytoplasmic proteins (**Supplementary Fig. 14B**). This suggests that *CD74* contributes to the normal function and expression of antigen-presenting proteins in macrophages.

Moreover, a greater number of DEGs were significantly downregulated in $RYR1^{+}ESRRG^{+}BICC1^{+}CD74^{+}$ macrophages in DN (Fig. 11A). These downregulated DEGs were notably enriched in signaling pathways related to the regulation of apoptosis, Th1/Th2 cell differentiation, receptor-mediated endocytosis, and protein ubiquitination, among others (Fig. 11B,C). This suggests that $APP^{+}GABBR1^{hi}CHRM3^{hi}$ cells regulated the translation and modification of macrophage proteins, phagocytic function, and cell survival in macrophages through *CD74*.

$RYR1^{+}ESRRG^{+}BICC1^{+}$ Macrophages Regulate Podocyte Injury Through SLIT2 and PDGF Signaling Pathways in Diabetic Nephropathy

Next, the role of the newly identified $RYR1^{+}ESRRG^{+}BICC1^{+}CD74^{+}$ macrophages phenotype in PODO injury in DN was investigated. Initially, a total of 2025 PODO were identified from the kidney tissues, characterized as $NPHS1^{hi}NPHS2^{hi}$, with a distribution of 812 in DN and 1213 in the CON group, and no significant difference in relative proportion was observed between groups (**Supplementary Fig. 2A**). Subsequently, we employed celltalker and cellphone analyses to assess the significance of ligand-receptor interactions between $RYR1^{+}ESRRG^{+}BICC1^{+}CD74^{+}$ macrophages and PODO. Results from celltalker indicated that $RYR1^{+}ESRRG^{+}BICC1^{+}CD74^{+}$ macrophages primarily interacted with PODO through *SLIT2* (mean_SCT = 0.223, $\log_2$FC = –1.305, $p < 0.05$), and *EFNA5* (mean_SCT = 0.085, $\log_2$FC = –0.737, $p < 0.05$), with interactions involving PODO surface *ROBO2* (mean_SCT = 0.900, $\log_2$FC = 0.447, $p < 0.001$), and *EPHA4* (mean_SCT = 0.089, $\log_2$FC = –0.093, $p < 0.001$) (**Supplementary Fig. 16**).

Furthermore, CellphoneDB complemented the above findings by demonstrating that $RYR1^{+}ESRRG^{+}BICC1^{+}CD74^{+}$ macrophages predominantly interacted with PODO through PDGFB (mean_SCT = 0.207, $\log_2$FC = –1.278, $p < 0.01$), which acted on the PODO surface receptor PDGFRB

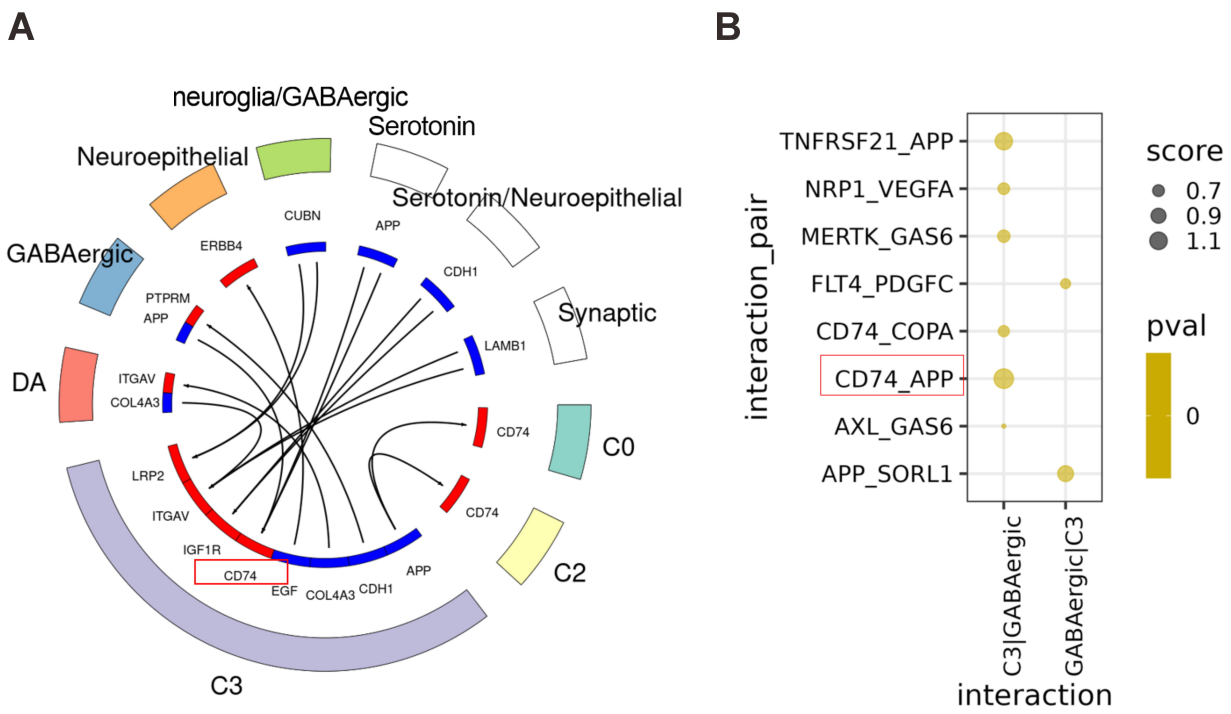

Fig. 8. Analysis of communication between C3 macrophages and different neuronal cell types. (A) The results of ligand-receptor interactions based on the celltalker method ($p < 0.05$, score >2). (B) Significance and strength of ligand-receptor interactions (CellphoneDB method, $p < 0.0001$).

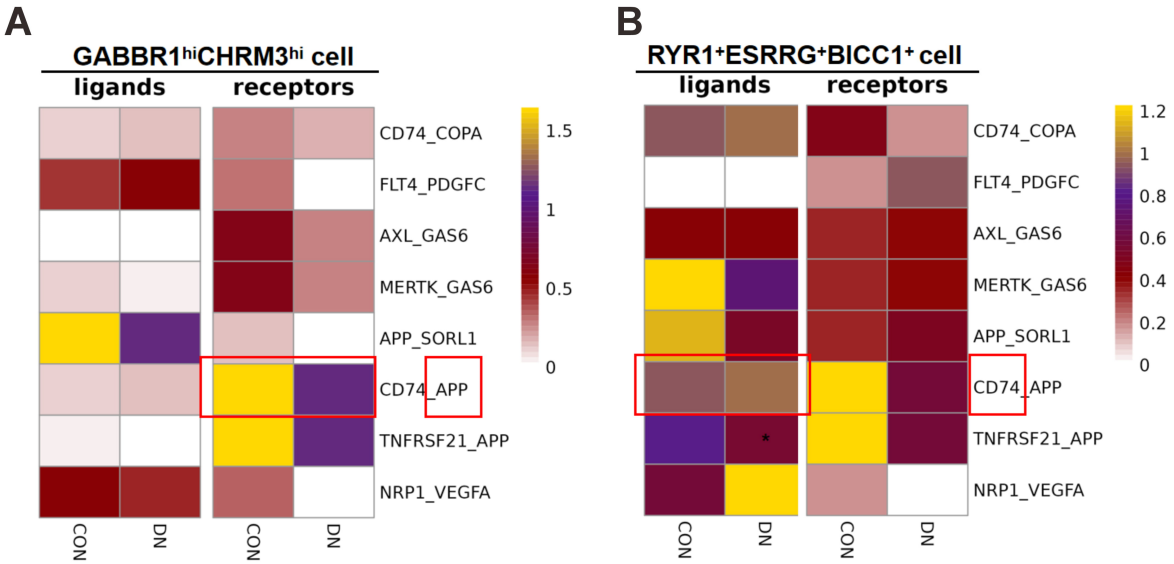

Fig. 9. Average expression levels of ligands and receptors in different samples. (A,B) The average expression levels of ligands and receptors (CellphoneDB results) in *GABBR1*^{hi}*CHRM3*^{hi} neuron-like cells (A) and *RYR1*$^{+}$*ESRRG*$^{+}$*BICC1*$^{+}$ macrophages (B) in the form of a heatmap. * indicates $p < 0.05$ compared to the CON group.

(mean_SCT = 0.258, $\log_2$FC = 0.144, $p < 0.01$) (Fig. 12). Furthermore, the expression of PDGFB in RYR1+ESRRG+BICC1+CD74+macrophages in DN was significantly reduced (Fig. 13).

Notably, *ROBO2* and *EPHA4* collectively regulated PODO foot processes, cell adhesion, and cell growth (**Supplementary Figs. 17,18**). This suggested that macrophages regulate the normal formation of PODO foot processes through *SLIT2-ROBO2* and *EFNA5-EPHA4* interactions. Downregulation of *SLIT2* and *EFNA5* expression in macrophages might lead to reduced levels of these molecules, which could impair the activation of *ROBO2* and *EPHA4*, resulting in PODO structural damage.

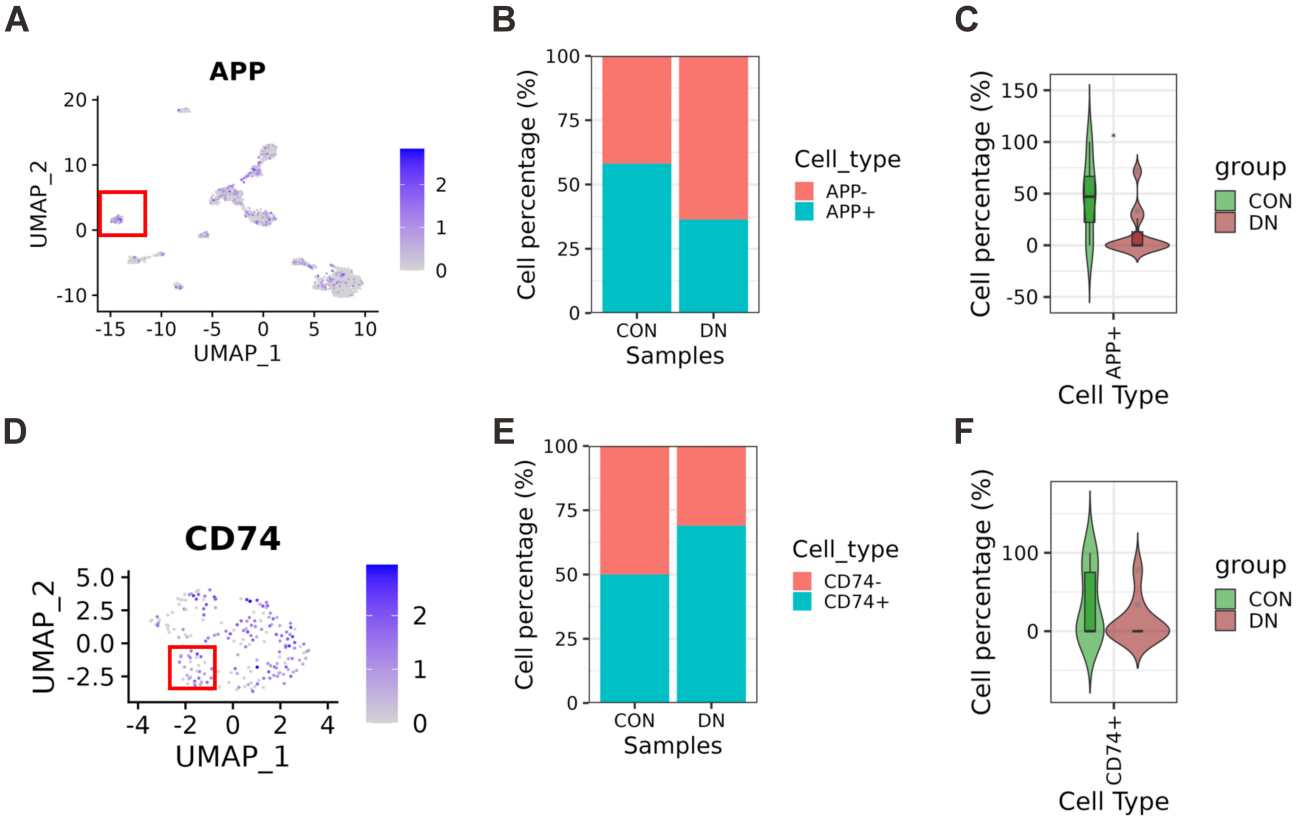

Fig. 10. Changes in the proportions of APP+ neurons and CD74+ macrophages. (A) The expression distribution of *APP* in renal neurons. (B,C) The relative proportion changes (B) and the significance of differences (C) of APP^{+} neurons in $GABBR1^{hi}CHRM3^{hi}$ cells between the control (CON) group and diabetic nephropathy (DN) tissue. (D) The expression distribution of *CD74* in macrophages. (E,F) The relative proportion changes (E) and the significance of differences (F) of $CD74^{+}$ macrophages in $RYR1^{+}ESRRG^{+}BICC1^{+}$ cells between the CON and DN groups. * indicates $p < 0.05$ compared to the CON group.

In addition, *PDGFRB* positively regulated the ECM components and cell size of PODO, indicating that the downregulation of *PDGFB* in macrophages might result in reduced *PDGFRB* activation, thereby disrupting PODO growth and morphology (Fig. 14A). *PDGFRB* signaling was also associated with pathways involving *PDGF* and *VEGFA-VEGFR2* in PODO (Fig. 14A).

Additionally, it was also found that $RYR1^{+}ESRRG^{+}BICC1^{+}CD74^{+}$ macrophages recognize *VEGFA* secreted by PODO through surface *NRP1/NRP2* (Fig. 12). Activation of *VEGFA* signaling via *NRP1/NRP2* was implicated in regulating signal transduction, cell chemotaxis, and proliferation in $RYR1^{+}ESRRG^{+}BICC1^{+}CD74^{+}$ macrophages (Fig. 14B). Overall, $RYR1^{+}ESRRG^{+}BICC1^{+}CD74^{+}$ macrophages reduce the inhibition of *PDGFRB* and downstream signaling in PODO through *PDGFB*. Simultaneously, weakened *PDGFRB* signaling inhibits the secretion of *VEGFA* by PODO. In turn, the decrease in *VEGFA* suppresses the functionality of $RYR1^{+}ESRRG^{+}BICC1^{+}CD74^{+}$ macrophages and their recruitment to the lesion site.

Podocytes Participate in Intracellular Signaling Regulation in $GABBR1^{hi}CHRM3^{hi}$ Cells Through the VEGFA-FLT1 Pathway in Diabetic Nephropathy

The analysis revealed the existence of signaling crosstalk between PODO and $GABBR1^{hi}CHRM3^{hi}$ cells in DN. Results from CellphoneDB analysis indicated that PODO primarily secreted various cytokines that acted on neuronal surface receptors, particularly through the *VEGFA-FLT1* and *UNC5D-NTN4* interactions (Fig. 15A–C). Furthermore, Celltalker results demonstrated that PODO secreted *PLG* and *CALM2*, which acted on *FLT1* and *INSR* receptors on $GABBR1^{hi}CHRM3^{hi}$ cells (**Supplementary Fig. 19A–C**).

In terms of gene expression, PODO exhibited a decrease in *PLG* ($p < 0.01$, **Supplementary Fig. 19C**), *VEGFA* ($p < 0.001$, Fig. 15C), *UNC5D* ($p < 0.001$, Fig. 15C), and an increase in *CALM2* ($p < 0.001$, **Supplementary Fig. 19C**). Specifically, *PLG* (mean_SCT = 0.051, $\log_2$FC = –0.120, $p < 0.001$), *VEGFA* (mean_SCT = 1.209, $\log_2$FC = –0.281, $p < 0.001$), *UNC5D* (mean_SCT = 0.493, $\log_2$FC = 0.992, $p < 0.001$), and *CALM2* (mean_SCT = 0.146, $\log_2$FC = 0.183, $p < 0.001$) were interacted with *FLT1* (mean_SCT = 0.815, $\log_2$FC = –1.163,

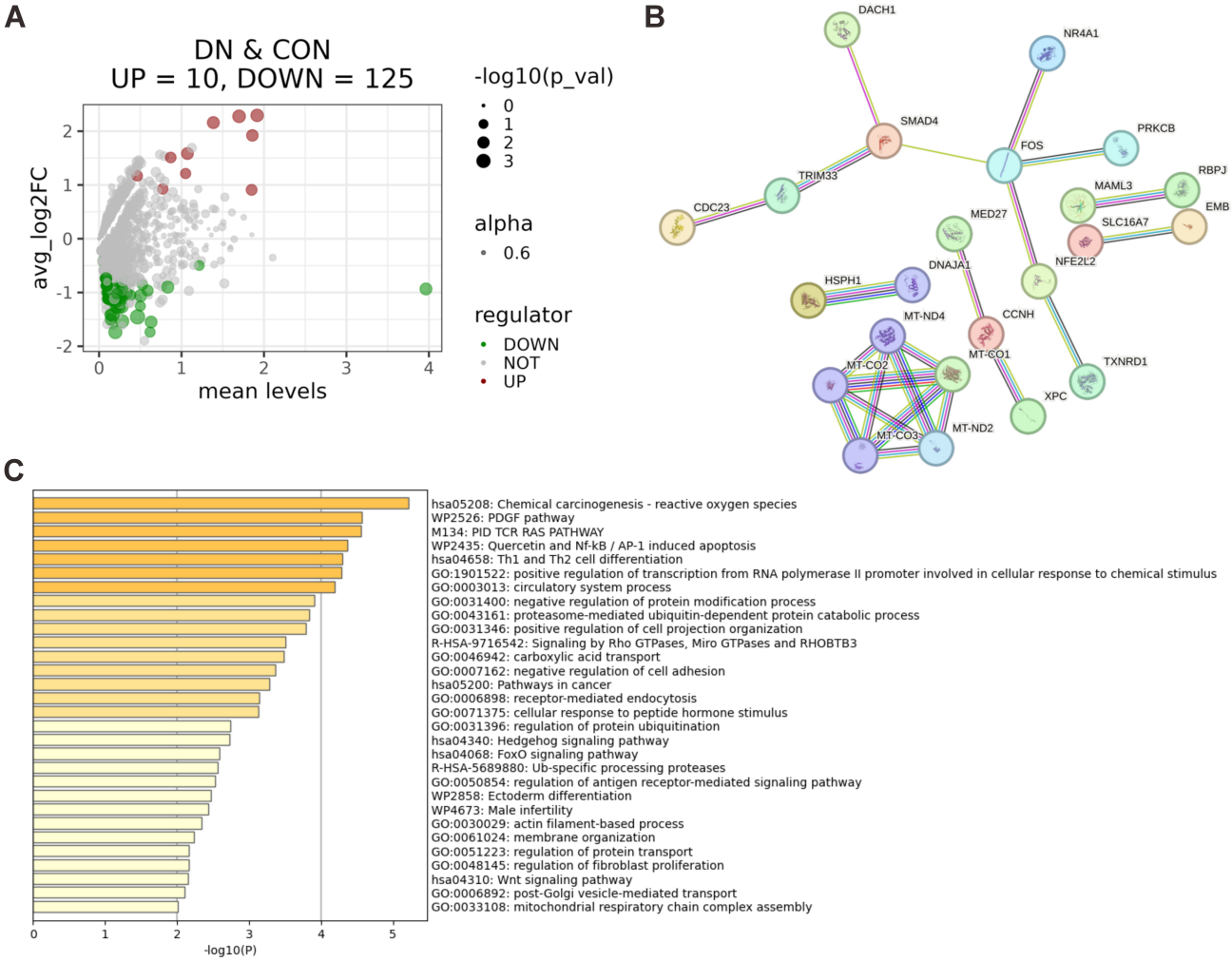

Fig. 11. Functional changes in *CD74*$^{+}$ macrophages in diabetic nephropathy. (A) A volcano plot displaying significantly differentially expressed genes (DEGs) in *CD74*$^{+}$ macrophages in DN. (B) Interaction network among DEGs. (C) The significantly enriched signaling pathways of DEGs.

$p < 0.001$), *NTN4* (mean_SCT = 0.093, $\log_2$FC = –1.253, $p < 0.05$), and *INSR* (mean_SCT = 0.544, $\log_2$FC = –0.933, $p < 0.05$) on the surface of *GABBR1*^{hi}*CHRM3*^{hi} cells, respectively.

Further functional analysis revealed that *FLT1* and *NTN4* were involved in regulating *MAPK* signaling and endocytosis in *GABBR1*^{hi}*CHRM3*^{hi} cells (Fig. 16). In addition, *INSR* was primarily involved in the FoxO signaling pathway, rheumatoid arthritis-related pathways, and the regulation of cellular catabolic metabolism functions (**Supplementary Fig. 20**). Notably, *VEGFA* and *FLT1* exhibited the highest expression levels in PODO and *GABBR1*^{hi}*CHRM3*^{hi} cells, suggesting their role as key proteins in the intercellular signaling between these two cell types. This indicates that in DN, PODO actively participate in regulating intracellular signal transmission and physiological functions in *GABBR1*^{hi}*CHRM3*^{hi} cells through the *VEGFA-FLT1* pathway. However, neuron-like cells might modulate PODO foot process morphology through *SLIT2* activation of *ROBO2*, although the expression levels of this signal did not differ significantly in DN (Fig. 15 and **Supplementary Fig. 21**).

In Vitro Validation of the Interaction Between APP and CD74

Finally, the interaction between APP and CD74 was validated *in vitro*. First, *GABBR1*^{hi}*CHRM3*^{hi} neuron-like cells were treated with high glucose (HG; 30 mM D-glucose) for 24 h. qRT-PCR results showed that HG treatment significantly downregulated APP expression in these cells (Fig. 16A), a finding that was further confirmed at the protein level by Western blot (Fig. 16B). Subsequently, the culture supernatant from HG-treated *GABBR1*^{hi}*CHRM3*^{hi} neuron-like cells (HG-CCS) was collected and added to *RYR1*$^{+}$*ESRRG*$^{+}$*BICC1*$^{+}$ macrophages for an additional 24 h incubation prior to harvest. Similarly, CD74 expression was downregulated in *RYR1*$^{+}$*ESRRG*$^{+}$*BICC1*$^{+}$ macrophages at both the mRNA

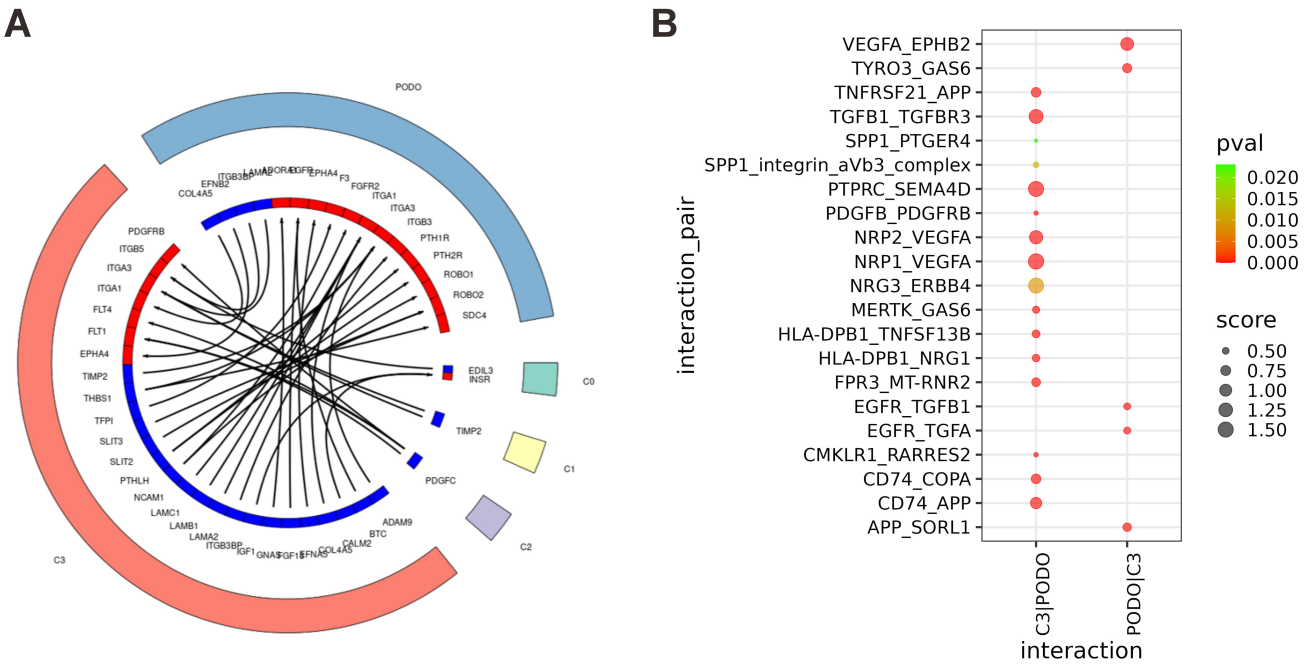

Fig. 12. Analysis of interactions between podocytes (PODO) and *RYR1*$^{+}$*ESRRG*$^{+}$*BICC1*$^{+}$macrophages. (A,B) Results of cell communication analysis using celltalker (A) and CellphoneDB (B).

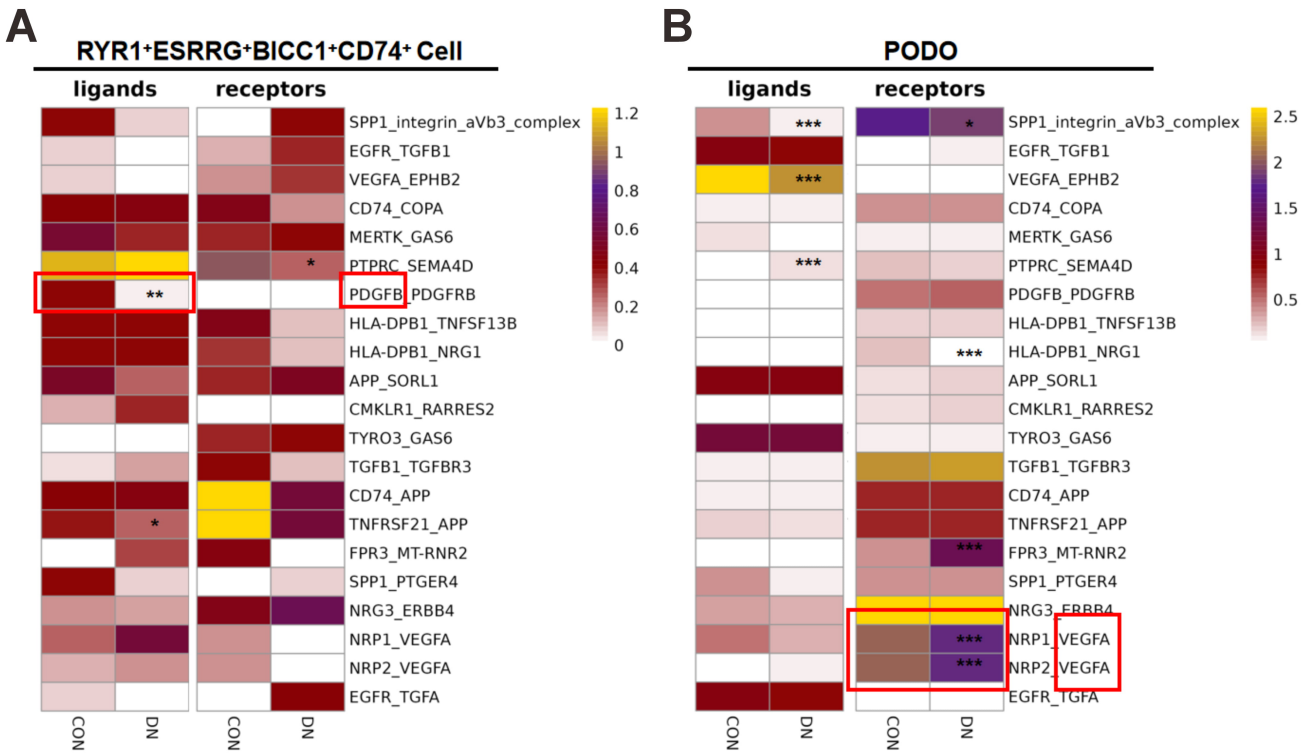

Fig. 13. Expression of ligands and receptors mediating interactions between podocytes (PODO) and macrophages. *, ** and *** indicate significance compared to the CON (control) group, with $p < 0.05$, $p < 0.01$ and $p < 0.001$, respectively. (A,B) The average expression levels of ligands and receptors in PODO (A) and macrophage (B) cell.

and protein levels (Fig. 16C,D). Flow cytometry analysis also confirmed a reduction in the number of CD74-positive macrophages (Fig. 16E). Co-immunoprecipitation (Co-IP) results demonstrated an interaction between APP and CD74 (Fig. 16F). Notably, this interaction was attenuated in macrophages treated with HG-CCS (Fig. 16F).

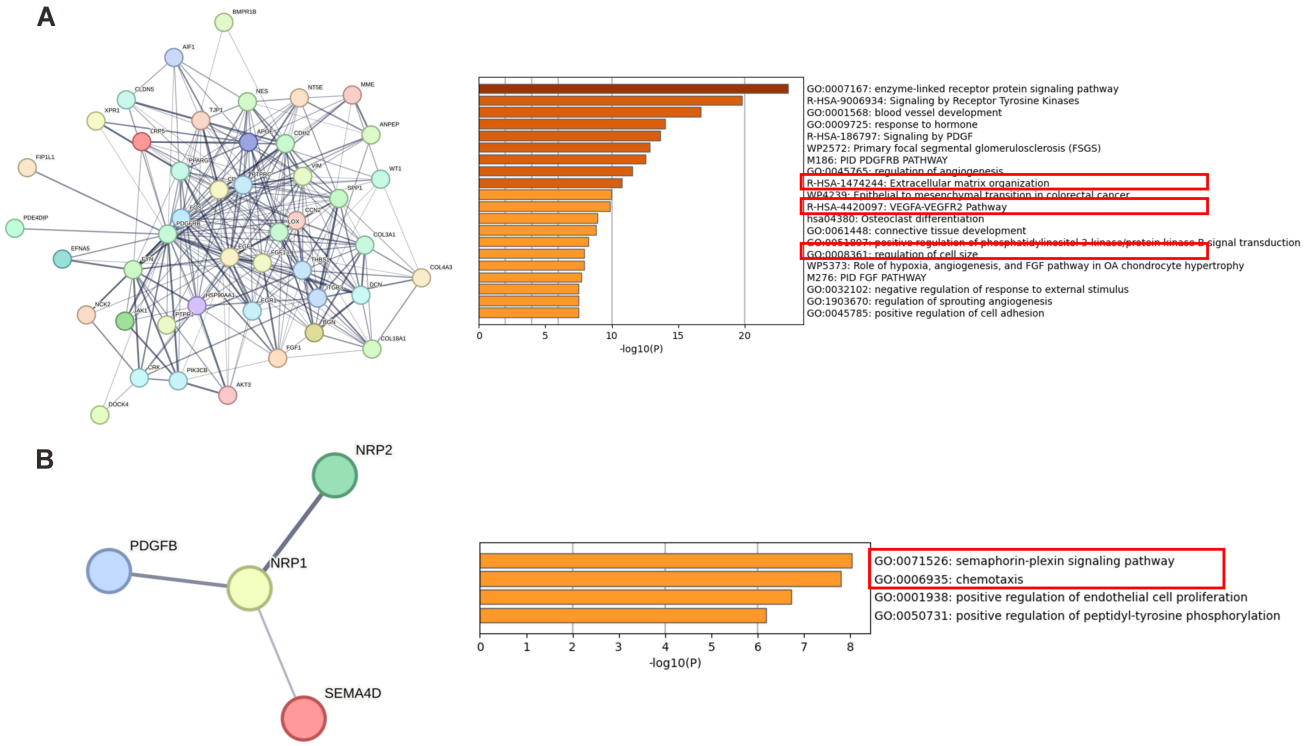

Fig. 14. Impact of intercellular signaling on podocytes (PODO) and *CD74*$^+$ macrophages functions. (A,B) The interactions of *PDGFRB* in PODO (A) and *NRP1/NRP2* in *CD74*$^+$ macrophages (B) with significantly differentially expressed genes and the signaling pathways enriched therein.

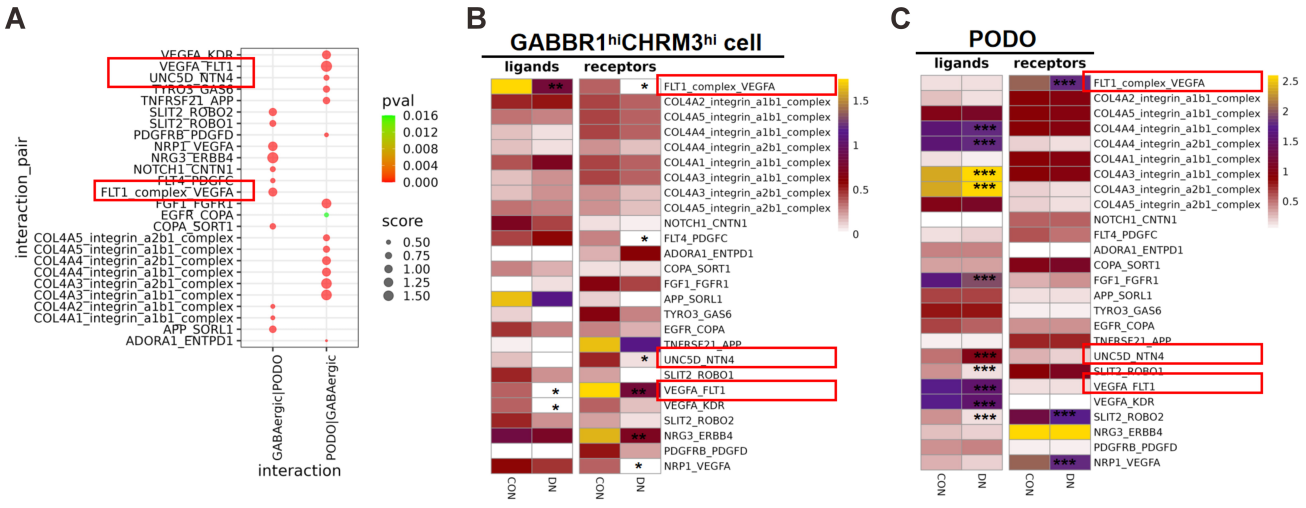

Fig. 15. CellphoneDB analysis identifies *VEGFA-FLT1* as the key signaling interaction between renal neurons and podocytes (PODO). (A) The scores for various ligand-receptor pairs involved in the interaction between renal neurons and PODO, as determined by CellphoneDB. (B) The expression patterns of key ligand-receptor pairs in renal neurons. (C) The expression patterns of key ligand-receptor pairs in PODO. *, **, *** indicate significance compared to the CON (control) group, with $p < 0.05$, $p < 0.01$, and $p < 0.001$, respectively.

Discussion

Activation of renal nerves leads to a reduction in efferent renal sympathetic nerve activity, resulting in an increased renal excretion of sodium in urine [22]. Studies on renal denervation have confirmed the regulatory role of nerves in immune inflammation and kidney damage, especially in conditions like hypertension and nephritis [22–25]. This regulation involves the release of neurotransmitters such as bradykinin, *SP*, Norepinephrine (NE), and CGRP in response to mechanical stimuli. *SP*, NE, and CGRP recruit

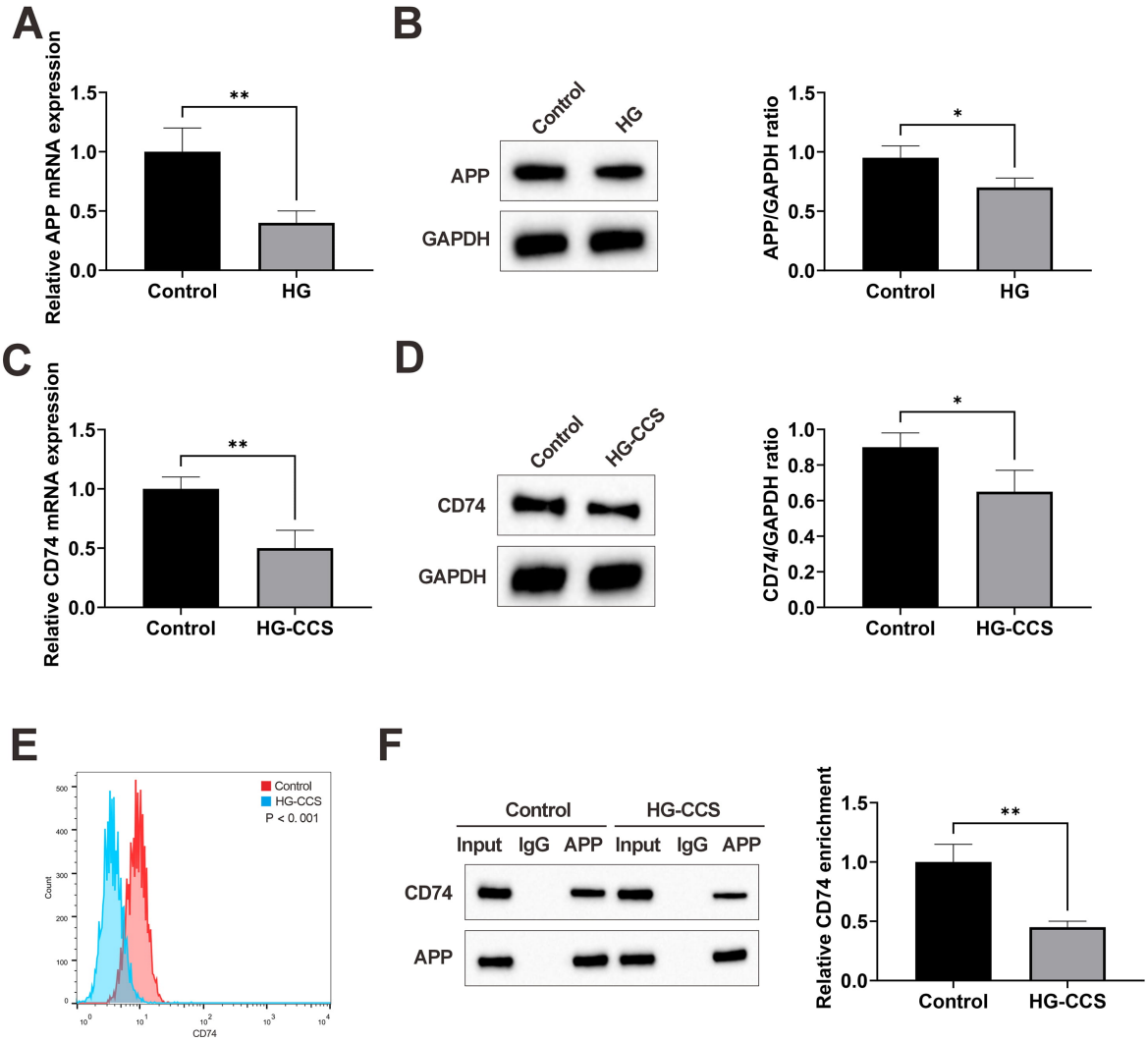

Fig. 16. *In Vitro* Validation of the Interaction Between APP and CD74. (A) qRT-PCR analysis of APP expression. (B) Western blot analysis of APP expression. (C) qRT-PCR analysis of CD74 expression. (D) Western blot analysis of CD74 expression. (E) Flow cytometric detection of CD74-positive macrophages. (F) Co-immunoprecipitation (Co-IP) analysis of the interaction between APP and CD74. *, ** indicate significant differences compared with the control group, with $p < 0.05$ and $p < 0.01$, respectively.

NK1R-positive and *ED1*-positive monocytes/macrophages, facilitating their infiltration into the kidney [26–29]. Additionally, these neurotransmitters induce macrophages to adopt an inflammatory phenotype, leading to the secretion of pro-inflammatory cytokines such as IL-1β, IL-6, IL-18, and TNF-α, thereby mediating neuroinflammation. This renal nerve-mediated immune signaling creates an unfavorable inflammatory environment in the kidneys, exacerbating renal damage. These findings emphasize the importance of not overlooking the role of renal nerves in kidney damage and their potential involvement in mediating inflammatory responses.

Clinical research has indicated that nerve damage is a risk factor for the development of DN, with common pathological mechanisms found between nerve injury diseases and DN [30,32–34]. Multiple studies have observed ultrastructural changes in the kidneys of diabetic rats, including the loss of nerve fibers, indicating that changes in the morphology and function of renal nerves play a role in the progression of DN [35,36]. This research detected a significant decrease in a specific type of neuron-like cells (*GABBR1*^{hi}*CHRM3*^{hi}) with abnormal gene expression related to neural apoptosis/survival pathways, suggesting abnormal neuronal apoptosis in DN. Concurrently, biological functions such as intercellular adhesion regulation among neuron-like cells were activated, implying that DN-related neuronal damage may mediate enhanced intercellular signal transmission. Neuronal damage in DN may be associated with a reduction in the secretion of *VEGFA* by PODO. Existing research has shown that PODO and neuron-like cells show overlapping distributions in the kidneys, with PODO possessing neuron-like projections that are regulated by neurotransmitters and cytokines secreted by neurons [37]. This study also reveals direct signal communica-

tion between PODO and renal neuron-like cells. However, in contrast to the findings, PODO secrete *VEGFA*, which interacts significantly with renal nerves via *FLT1*. Loss of *FLT1* renders neurons more susceptible to stress, leading to induced apoptosis [38,39]. Conversely, activation of *FLT1* by *VEGFA* promotes in neuronal survival. The weakened interaction between *VEGFA* and *FLT1* in DN may be a key factor in renal neuronal damage.

In renal injury research, there is increasing evidence that neurons release cytokines, which play a role in regulating renal cell damage and IMC activation, as observed with *SP* and CGRP. This study primarily focused on the signal communication between renal nerves and macrophages. In most chronic renal injury models, including DN, renal nerves have been found to recruit macrophages, leading to their significant infiltration in kidney tissues and subsequent mediation of inflammation. However, in the present study, which analyzed human DN kidney tissue *via* scRNA-seq found a significant decrease in the relative proportion of macrophages ($p < 0.05$). This discrepancy can be attributed to several factors. For example, the pronounced infiltration of macrophages is mainly evident in animal models, whereas the number of macrophages in DN varies dynamically across different stages of the disease. In the early stages of DN, macrophages are activated by damage-associated molecular patterns to adopt an M2-like phenotype, which facilitates the phagocytosis of damaged cells, resistance to inflammation, and tissue repair. As the disease progresses, M2 macrophages are depleted, becoming incapable of repairing tissue, and the increase in pro-inflammatory factors leads to the recruitment of peripheral blood monocytes, thus exacerbating renal inflammatory damage [16–18]. Another explanation for these findings is that there are primarily two sources of renal macrophages, each with different roles in DN [16–18]. Most current research has concentrated on monocyte-derived macrophages, identified by markers for monocytes or classical bifurcated macrophages. However, these markers do not fully represent all types of renal macrophages. In reality, the predominant type of renal macrophage is TMs. Through transcriptomic analysis of macrophage expression characteristics, the present study revealed that renal macrophages mainly express *PTPRC*, displaying different transcriptional characteristics and markers from those of monocyte-derived macrophages ($CD14^{+}LYZ^{+}$). Trajectory analysis indicated that the identified macrophages were derived from embryonic kidney cells, suggesting that the macrophages identified could be classified as TM. Further subtyping analysis identified four main types of macrophages in DN, among which the C3 subtype ($RYR1^{+}ESRRG^{+}BICC1^{+}$) represented differentiated mature macrophages, characterized by significantly reduced transcriptomic expression scores in inflammation regulation pathways. Additionally, their similarity to classical bifurcated macrophages was assessed by examining the expression of classic markers including *CD86*, *CD163*, and *MRC1*. The results showed that C3 macrophages expressed *CD163* and *MRC1* at higher levels compared to other subtypes, suggesting that C3 macrophages may play an anti-inflammatory role similar to that of typical M2 macrophages, which are known to secrete anti-inflammatory factors like IL-10, thereby reducing the inflammatory response. However, in DN, the proportion of C3 macrophages significantly decreases, implying that the depletion of $RYR1^{+}ESRRG^{+}BICC1^{+}$ macrophages impaired the normal suppression of renal cell damage-mediated inflammatory responses, thereby exacerbating kidney injury. In DN, it is primarily the renal nerves that communicate with TMs.

Research conducted by Qian Z and colleagues has confirmed that renal neurons communicate with TMs [30], although the specific nature of these signals was not fully elucidated. Cell communication analysis in the present study unveiled a novel type of interaction signal between the two cell types: *APP-CD74*. *APP*, first discovered in the context of Alzheimer's disease [40], is an amyloid protein secreted by $GABBR1^{hi}CHRM3^{hi}$ cells and PODO, and interacts with *CD74* on the surface of immune cells, promoting Th17 differentiation and macrophage migration to injury sites [41]. CD74 is a non-polymorphic type II transmembrane glycoprotein with various biological functions in physiological and pathological states [42]. Once activated within the cell, *CD74* facilitates the reassembly and membrane localization of MHCII molecules [43]. As a transcriptional regulatory factor, *CD74* also modulates the expression of genes related to proliferation and apoptosis, impacting cell survival [44,45]. In DN, abnormal *CD74* signaling in $RYR1^{+}ESRRG^{+}BICC1^{+}$ macrophages is involved in participates in phagocytosis and aids in T-cell differentiation. However, the expression of *APP* in renal $GABBR1^{hi}CHRM3^{hi}$ cells is reduced, indicating a weakened interaction between $GABBR1^{hi}CHRM3^{hi}$ cells and $RYR1^{+}ESRRG^{+}BICC1^{+}$ macrophages via the *APP-CD74* axis. This leads to aberrant intracellular signaling in macrophages, promoting apoptosis.

In DN, the function and polarization of macrophages are regulated by renal cells, particularly PODO. PODO secrete *MIF* that targets and binds to *CD74* on macrophages, mediating inflammatory responses [46]. Conversely, cytokines secreted by macrophages, such as IL-2 and TNF-α, have been implicated in PODO damage [12,13]. Macrophages play a crucial role as key regulatory IMC in PODO injury. This study revealed that the interaction between PODO and $RYR1^{+}ESRRG^{+}BICC1^{+}$ macrophages in DN, specifically involving *VEGFA-NRP1* and *VEGFA-NRP2* pathways, was diminished. This observation suggests that under normal condition, PODO secrete *VEGFA*, which stimulates renal macrophages via *NRP1/2* on their surface. Research confirms that *NRP1/2* are associated with the anti-inflammatory function of macrophages [47,48].

This indicates that PODO damage in DN leads to reduced levels of *VEGFA* in the renal environment, thereby suppressing the anti-inflammatory function of macrophages. Furthermore, the depletion of *RYR1*$^{+}$*ESRRG*$^{+}$*BICC1*$^{+}$ macrophages in DN weakens their interaction with PODO via the *SLIT2-ROBO2*, *EFNA5-EPHA4*, and *PDGFB-PDGFRB* signaling pathways. *ROBO2* and *EPHA4* are genes that promote axonal formation. Reduced expression of *ROBO2* and *EPHA4* in PODO might lead to the loss of foot processes, contributing to PODO injury, and apoptosis [49,50]. Conversely, upregulating *ROBO2* and *EPHA4* *in vitro* promotes the formation of normal PODO morphology. This indicates that reduced expression of *SLIT2* and *EFNA5* in *RYR1*$^{+}$*ESRRG*$^{+}$*BICC1*$^{+}$ macrophages may lead to decreased activation of *ROBO2* and *EPHA4*, adversely affecting the formation of PODO foot processes. Additionally, the weakened interaction between *PDGFB* and *PDGFRB* in PODO, which is related to cell growth, may result in suppressed cell growth [51]. *PDGFRB* also regulates downstream *VEGFA-VEGFR2* signaling, and its reduced expression or weakened function further diminishes *VEGFA* survival, adversely affecting the anti-inflammatory and antigen-presenting functions of renal macrophages.

This study has several limitations. First, the conclusions are based on the mining and analysis of publicly available online data and have not yet been validated through *in vitro* cellular experiments or *in vivo* animal studies; thus, the reliability and generalizability of the findings require further confirmation. Second, the crosstalk mechanisms among the *VEGFA-NRP1/NRP2*, *SLIT2-ROBO2*, *EFNA5-EPHA4*, and *PDGFB-PDGFRB* signaling pathways were not thoroughly explored. The synergistic or antagonistic roles of these pathways within the "renal neuron–macrophage–podocyte" interaction network remain to be elucidated in future research. Additionally, renal innervation comprises both sympathetic and parasympathetic systems. Existing studies indicate that the sympathetic system promotes inflammation by releasing catecholamines, which activate adrenergic receptors on immune cells, whereas the parasympathetic system exerts anti-inflammatory effects via the cholinergic anti-inflammatory pathway mediated by the vagus nerve [52]. However, scRNA-seq/snRNA-seq techniques are unable to precisely identify renal neurons and nerve fibers. This study could only identify neuron-like cells involved in neural signaling, without clarifying their specific cellular subtypes. Consequently, the investigation of communication between renal nerves and renal parenchymal cells, including macrophages, remains indirect.

Conclusion

In DN, there is dynamic communication between renal neuron-like cells, resident macrophages and PODO.

Availability of Data and Materials

All of DN-related snRNA-seq (GSE131882, GSE151302, GSE195460, GSE118184, GSE114156) and neurons-related scRNA-seq (GSE209947, GSE192405, GSE213569) data can be found in GEO database (https://www.ncbi.nlm.nih.gov/gds/). And PBMC related scRNA-seq data can be obtained from 10x genomics database (https://cf.10xgenomics.com/samples/cell/pbmc3k/pbmc3k_filtered_gene_bc_matrices.tar.gz, https://cf.10xgenomics.com/samples/cell/pbmc4k/pbmc4k_filtered_gene_bc_matrices.tar.gz).

Author Contributions

JL and YLZ conceptualized the study; HYL and WF curated the data; ZPQ and HHC performed the formal analysis; XFW and JEK conducted the investigation; HQQ and XXM developed the methodology; JL and YLZ wrote the original draft; XXM reviewed and critically edited the manuscript, and other authors made important revisions to the original manuscript. All authors have read and agreed to the published version of the manuscript. All authors have participated sufficiently in the work to take public responsibility for appropriate portions of the content and agreed to be accountable for all aspects of the work in ensuring that questions related to its accuracy or integrity.

Ethics Approval and Consent to Participate

Not applicable.

Acknowledgment

Not applicable.

Funding

(1) Municipality and Mniversity Joint Project of Guangzhou Science and Technology Bureau (No.2023A03J0307); (2) Major Project of The Affiliated TCM Hospital of Guangzhou Medical University (No.20210146).

Conflict of Interest

The authors declare no conflict of interest.

Supplementary Material

Supplementary material associated with this article can be found, in the online version, at https://doi.org/10.24976/Discov.Med.202638207.98.

References

[1] Perkovic V, Jardine MJ, Neal B, Bompoint S, Heerspink HJL, Charytan DM, *et al*. Canagliflozin and Renal Outcomes in Type 2 Diabetes and Nephropathy. The New England Journal of Medicine. 2019; 380: 2295–2306. https://doi.org/10.1056/NEJMoa1811744.

[2] Li X, Zhang Y, Xing X, Li M, Liu Y, Xu A, *et al*. Podocyte injury of diabetic nephropathy: Novel mechanism discovery and therapeutic prospects. Biomedicine & Pharmacotherapy. 2023; 168: 115670. https://doi.org/10.1016/j.biopha.2023.115670.

[3] Zhao Y, Fan S, Zhu H, Zhao Q, Fang Z, Xu D, *et al*. Podocyte OTUD5 alleviates diabetic kidney disease through deubiquitinating TAK1 and reducing podocyte inflammation and injury. Nature Communications. 2024; 15: 5441. https://doi.org/10.1038/s41467-024-49854-1.

[4] Reynolds PA. The mechanobiology of kidney podocytes in health and disease. Clinical Science (London, England: 1979). 2020; 134: 1245–1253. https://doi.org/10.1042/CS20190764.

[5] Guo Y, Song Z, Zhou M, Yang Y, Zhao Y, Liu B, *et al*. Infiltrating macrophages in diabetic nephropathy promote podocytes apoptosis via TNF-α-ROS-p38MAPK pathway. Oncotarget. 2017; 8: 53276–53287. https://doi.org/10.18632/oncotarget.18394.

[6] Li HD, You YK, Shao BY, Wu WF, Wang YF, Guo JB, *et al*. Roles and crosstalks of macrophages in diabetic nephropathy. Frontiers in Immunology. 2022; 13: 1015142. https://doi.org/10.3389/fimmu.2022.1015142.

[7] Espinel E, Agraz I, Ibernon M, Ramos N, Fort J, Serón D. Renal Biopsy in Type 2 Diabetic Patients. Journal of Clinical Medicine. 2015; 4: 998–1009. https://doi.org/10.3390/jcm4050998.

[8] Awad AS, You H, Gao T, Cooper TK, Nedospasov SA, Vacher J, *et al*. Macrophage-derived tumor necrosis factor-α mediates diabetic renal injury. Kidney International. 2015; 88: 722–733. https://doi.org/10.1038/ki.2015.162.

[9] Calle P, Hotter G. Macrophage Phenotype and Fibrosis in Diabetic Nephropathy. International Journal of Molecular Sciences. 2020; 21: 2806. https://doi.org/10.3390/ijms21082806.

[10] Chebotareva NV, Bobkova IN, Lysenko LV. The role of podocytes dysfunction in chronic glomerulonephritis progression. Terapevticheskii Arkhiv. 2018; 90: 92–97. https://doi.org/10.26442/terarkh201890692-97.

[11] Ishikawa Y, Gohda T, Tanimoto M, Omote K, Furukawa M, Yamaguchi S, *et al*. Effect of exercise on kidney function, oxidative stress, and inflammation in type 2 diabetic KK-A(y) mice. Experimental Diabetes Research. 2012; 2012: 702948. https://doi.org/10.1155/2012/702948.

[12] Qu Z, Chu J, Jin S, Yang C, Zang J, Zhang J, *et al*. Tissue-resident macrophages and renal diseases: landscapes and treatment directions. Frontiers in Immunology. 2025; 16: 1548053. https://doi.org/10.3389/fimmu.2025.1548053.

[13] Tang PMK, Nikolic-Paterson DJ, Lan HY. Macrophages: versatile players in renal inflammation and fibrosis. Nature Reviews. Nephrology. 2019; 15: 144–158. https://doi.org/10.1038/s41581-019-0110-2.

[14] Liu F, Dai S, Feng D, Qin Z, Peng X, Sakamuri SSVP, *et al*. Distinct fate, dynamics and niches of renal macrophages of bone marrow or embryonic origins. Nature Communications. 2020; 11: 2280. https://doi.org/10.1038/s41467-020-16158-z.

[15] Sears SM, Vega AA, Kurlawala Z, Oropilla GB, Krueger A, Shah PP, *et al*. F4/80^{hi} Resident Macrophages Contribute to Cisplatin-Induced Renal Fibrosis. Kidney360. 2022; 3: 818–833. https://doi.org/10.34067/KID.0006442021.

[16] Zimmerman KA, Song CJ, Li Z, Lever JM, Crossman DK, Rains A, *et al*. Tissue-Resident Macrophages Promote Renal Cystic Disease. Journal of the American Society of Nephrology: JASN. 2019; 30: 1841–1856. https://doi.org/10.1681/ASN.2018080810.

[17] Meng XM, Mak TSK, Lan HY. Macrophages in Renal Fibrosis. Advances in Experimental Medicine and Biology. 2019; 1165: 285–303. https://doi.org/10.1007/978-981-13-8871-2_13.

[18] Wen Y, Crowley SD. The varying roles of macrophages in kidney injury and repair. Current Opinion in Nephrology and Hypertension. 2020; 29: 286–292. https://doi.org/10.1097/MNH.0000000000000595.

[19] Deng S, Zhou X, Ge Z, Song Y, Wang H, Liu X, *et al*. Exosomes from adipose-derived mesenchymal stem cells ameliorate cardiac damage after myocardial infarction by activating S1P/SK1/S1PR1 signaling and promoting macrophage M2 polarization. The International Journal of Biochemistry & Cell Biology. 2019; 114: 105564. https://doi.org/10.1016/j.biocel.2019.105564.

[20] Yaghobian D, Don AS, Yaghobian S, Chen X, Pollock CA, Saad S. Increased sphingosine 1-phosphate mediates inflammation and fibrosis in tubular injury in diabetic nephropathy. Clinical and Experimental Pharmacology & Physiology. 2016; 43: 56–66. https://doi.org/10.1111/1440-1681.12494.

[21] Chen CA, Chang JM, Yang YL, Chang EE, Chen HC. Macrophage migration inhibitory factor regulates integrin-β1 and cyclin D1 expression via ERK pathway in podocytes. Biomedicine & Pharmacotherapy. 2020; 124: 109892. https://doi.org/10.1016/j.biopha.2020.109892.

[22] Kopp UC. Role of renal sensory nerves in physiological and pathophysiological conditions. American Journal of Physiology. Regulatory, Integrative and Comparative Physiology. 2015; 308: R79–R95. https://doi.org/10.1152/ajpregu.00351.2014.

[23] Böhner AMC, Jacob AM, Heuser C, Stumpf NE, Effland A, Abdullah Z, *et al*. Renal Denervation Exacerbates LPS- and Antibody-induced Acute Kidney Injury, but Protects from Pyelonephritis in Mice. Journal of the American Society of Nephrology: JASN. 2021; 32: 2445–2453. https://doi.org/10.1681/ASN.2021010110.

[24] Xiao L, Kirabo A, Wu J, Saleh MA, Zhu L, Wang F, *et al*. Renal Denervation Prevents Immune Cell Activation and Renal Inflammation in Angiotensin II-Induced Hypertension. Circulation Research. 2015; 117: 547–557. https://doi.org/10.1161/CIRCRESAHA.115.306010.

[25] Veelken R, Vogel EM, Hilgers K, Amann K, Hartner A, Sass G, *et al*. Autonomic renal denervation ameliorates experimental glomerulonephritis. Journal of the American Society of Nephrology: JASN. 2008; 19: 1371–1378. https://doi.org/10.1681/ASN.2007050552.

[26] Zou X, Lin S, Zhong L, Liu J, Meng Y, Zhu Y, *et al*. Renal denervation alleviates renal ischemic reperfusion injury-induced acute and chronic kidney injury in rats partly by modulating miRNAs. Clinical and Experimental Nephrology. 2022; 26: 13–21. https://doi.org/10.1007/s10157-021-02129-1.

[27] McMaster WG, Kirabo A, Madhur MS, Harrison DG. Inflammation, immunity, and hypertensive end-organ damage. Circulation Research. 2015; 116: 1022–1033. https://doi.org/10.1161/CIRCRESAHA.116.303697.

[28] Rodionova K, Hilgers KF, Linz P, Schätzl J, Raschke G, Ott C, *et al*. Neurogenic substance P-influences on action potential production in afferent neurons of the kidney? Pflugers Archiv: European Journal of Physiology. 2021; 473: 633–646. https://doi.org/10.1007/s00424-021-02552-z.

[29] Rodionova K, Hilgers KF, Paulus EM, Tiegs G, Ott C, Schmieder R, *et al*. Neurogenic tachykinin mechanisms in experimental nephritis of rats. Pflugers Archiv: European Journal of Physiology. 2020; 472: 1705–1717. https://doi.org/10.1007/s00424-020-02469-z.

[30] Zhu Q, Xiao L, Cheng G, He J, Yin C, Wang L, *et al*. Self-

maintaining macrophages within the kidney contribute to salt and water balance by modulating kidney sympathetic nerve activity. Kidney International. 2023; 104: 324–333. https://doi.org/10.1016/j.kint.2023.04.023.

[31] Yang Z, Lou X, Zhang J, Nie R, Liu J, Tu P, *et al*. Association Between Early Markers of Renal Injury and Type 2 Diabetic Peripheral Neuropathy. Diabetes, Metabolic Syndrome and Obesity: Targets and Therapy. 2021; 14: 4391–4397. https://doi.org/10.2147/DMSO.S335283.

[32] Lytvyn Y, Albakr R, Bjornstad P, Lovblom LE, Liu H, Lovshin JA, *et al*. Renal hemodynamic dysfunction and neuropathy in longstanding type 1 diabetes: Results from the Canadian study of longevity in type 1 diabetes. Journal of Diabetes and its Complications. 2022; 36: 108320. https://doi.org/10.1016/j.jdiacomp.2022.108320.

[33] Firdous S, Wagai GA, Sharma K. A survey on diabetes risk prediction using machine learning approaches. Journal of Family Medicine and Primary Care. 2022; 11: 6929–6934. https://doi.org/10.4103/jfmpc.jfmpc_502_22.

[34] Asmy VKSS, Natarajan J. Comparative co-expression analysis of RNA-Seq transcriptome revealing key genes, miRNA and transcription factor in distinct metabolic pathways in diabetic nerve, eye, and kidney disease. Genomics & Informatics. 2022; 20: e26. https://doi.org/10.5808/gi.22029.

[35] Sato KL, Sanada LS, Ferreira RDS, de Marco MCDBDBO, Castania JA, Salgado HC, *et al*. Renal nerve ultrastructural alterations in short term and long term experimental diabetes. BMC Neuroscience. 2014; 15: 5. https://doi.org/10.1186/1471-2202-15-5.

[36] Kobayashi N, Gao SY, Chen J, Saito K, Miyawaki K, Li CY, *et al*. Process formation of the renal glomerular podocyte: is there common molecular machinery for processes of podocytes and neurons? Anatomical Science International. 2004; 79: 1–10. https://doi.org/10.1111/j.1447-073x.2004.00066.x.

[37] Dhondt J, Peeraer E, Verheyen A, Nuydens R, Buysschaert I, Poesen K, *et al*. Neuronal FLT1 receptor and its selective ligand VEGF-B protect against retrograde degeneration of sensory neurons. FASEB Journal: Official Publication of the Federation of American Societies for Experimental Biology. 2011; 25: 1461–1473. https://doi.org/10.1096/fj.10-170944.

[38] Wild R, Klems A, Takamiya M, Hayashi Y, Strähle U, Ando K, *et al*. Neuronal sFlt1 and Vegfaa determine venous sprouting and spinal cord vascularization. Nature Communications. 2017; 8: 13991. https://doi.org/10.1038/ncomms13991.

[39] Dunot J, Ribera A, Pousinha PA, Marie H. Spatiotemporal insights of APP function. Current Opinion in Neurobiology. 2023; 82: 102754. https://doi.org/10.1016/j.conb.2023.102754.

[40] Wan Y, Jiang J, Chen M, Han X, Zhong L, Xiao F, *et al*. Unravelling the imbalanced Th17-like cell differentiation by single-cell RNA sequencing in multiple myeloma. International Immunopharmacology. 2023; 124: 110852. https://doi.org/10.1016/j.intimp.2023.110852.

[41] Su H, Na N, Zhang X, Zhao Y. The biological function and significance of CD74 in immune diseases. Inflammation Research. 2017; 66: 209–216. https://doi.org/10.1007/s00011-016-0995-1.

[42] Schröder B. The multifaceted roles of the invariant chain CD74–More than just a chaperone. Biochimica et Biophysica Acta. 2016; 1863: 1269–1281. https://doi.org/10.1016/j.bbamcr.2016.03.026.

[43] Gil-Yarom N, Radomir L, Sever L, Kramer MP, Lewinsky H, Bornstein C, *et al*. CD74 is a novel transcription regulator. Proceedings of the National Academy of Sciences of the United States of America. 2017; 114: 562–567. https://doi.org/10.1073/pnas.1612195114.

[44] Valiño-Rivas L, Baeza-Bermejillo C, Gonzalez-Lafuente L, Sanz AB, Ortiz A, Sanchez-Niño MD. CD74 in Kidney Disease. Frontiers in Immunology. 2015; 6: 483. https://doi.org/10.3389/fimmu.2015.00483.

[45] Sanchez-Niño MD, Sanz AB, Ruiz-Andres O, Poveda J, Izquierdo MC, Selgas R, *et al*. MIF, CD74 and other partners in kidney disease: tales of a promiscuous couple. Cytokine & Growth Factor Reviews. 2013; 24: 23–40. https://doi.org/10.1016/j.cytogfr.2012.08.001.

[46] Wen E, Xin G, Li S, Dong Y, Zhu Y, Wan C, *et al*. Tuftsin ameliorates splenic inflammatory injury by promoting neuropilin-1 in severe acute pancreatitis. Biochemical Pharmacology. 2022; 199: 115030. https://doi.org/10.1016/j.bcp.2022.115030.

[47] Li T, Ran J, Miao Z, Yang M, Mou D, Jiang Y, *et al*. Deficiency of inflammation-sensing protein neuropilin-2 in myeloid-derived macrophages exacerbates colitis via NF-κB activation. The Journal of Pathology. 2024; 262: 175–188. https://doi.org/10.1002/path.6221.

[48] Bondeva T, Wolf G. Role of Neuropilin-1 in Diabetic Nephropathy. Journal of Clinical Medicine. 2015; 4: 1293–1311. https://doi.org/10.3390/jcm4061293.

[49] Fan X, Li Q, Pisarek-Horowitz A, Rasouly HM, Wang X, Bonegio RG, *et al*. Inhibitory effects of Robo2 on nephrin: a crosstalk between positive and negative signals regulating podocyte structure. Cell Reports. 2012; 2: 52–61. https://doi.org/10.1016/j.celrep.2012.06.002.

[50] Walkenhorst J, Dütting D, Handwerker C, Huai J, Tanaka H, Drescher U. The EphA4 receptor tyrosine kinase is necessary for the guidance of nasal retinal ganglion cell axons in vitro. Molecular and Cellular Neurosciences. 2000; 16: 365–375. https://doi.org/10.1006/mcne.2000.0878.

[51] Jia T, Xu T, Smeets B, Buhl EM, Moeller MJ, Floege J, *et al*. The Role of Platelet-Derived Growth Factor in Focal Segmental Glomerulosclerosis. Journal of the American Society of Nephrology: JASN. 2023; 34: 241–257. https://doi.org/10.1681/ASN.2022040491.

[52] Zoccali C, Mallamaci F, Kanbay M, Tuttle KR, Kotanko P, De Caterina R, *et al*. The autonomic nervous system and inflammation in chronic kidney disease. Nephrology, Dialysis, Transplantation: Official Publication of the European Dialysis and Transplant Association - European Renal Association. 2025; 40: 1470–1482. https://doi.org/10.1093/ndt/gfaf020.